Title

Cholinergic neurotransmission controls orexigenic endocannabinoid signaling in the gut in diet-induced obesity.

Journal

Journal of Neuroscience, 44(20)

ISSN

0270-6474

Authors

Wood, Courtney P

Alvarez, Camila

DiPatrizio, Nicholas V

Publication Date

2024-04-09

DOI

10.1523/jneurosci.0813-23.2024

Peer reviewed

The Journal of Neuroscience

https://jneurosci.msubmit.net

JN-RM-0813-23R1

Cholinergic neurotransmission controls orexigenic endocannabinoid signaling in the gut in diet-induced obesity

Nicholas DiPatrizio, University of California Riverside School of Medicine
Courtney Wood, University of California San Diego
Camila Alvarez, University of California Riverside

Commercial Interest:

Cholinergic neurotransmission controls orexigenic endocannabinoid signaling in the gut in diet-induced obesity

Abbreviated Title: Cholinergics drive eCB synthesis in obesity

Courtney P. Wood, Camila Alvarez, Nicholas V. DiPatrizio

Division of Biomedical Sciences, School of Medicine, University of California, Riverside, Riverside, CA, 92521, USA; University of California Riverside Center for Cannabinoid Research, Riverside, CA, 92521, USA

Corresponding Author: Nicholas V. DiPatrizio, ndipatri@medsch.ucr.edu

Number of Pages: 25

Number of Figures: 10

Number of Tables: 2

Number of Words for Abstract: 250

Number of Words for Introduction: 636

Number of Words for Discussion: 1,458

Conflict of Interest Statement: The authors declare no competing financial interests.

Acknowledgements: Research is funded by the National Institutes of Health (R01 DK119498 and L30 DK1149978) and the Tobacco-Related Disease Research Program (T29KT0232). The authors thank Samantha Sutley-Koury and Dr. Iryna Ethell's laboratory for their guidance in developing the cFos IHC assay, as well as Jeffrey Koury and Dr. Marcus Kaul's laboratory for training and use of the fluorescence microscope, and Will Cruz for assistance with chemical analyses.

Abstract

The brain bidirectionally communicates with the gut to control food intake and energy balance, which becomes dysregulated in obesity. For example, endocannabinoid (eCB) signaling in the small-intestinal epithelium (SI) is upregulated in diet-induced obese mice (DIO) and promotes overeating by a mechanism that includes inhibiting gut-brain satiation signaling. Upstream neural and molecular mechanism(s) involved in overproduction of orexigenic gut eCBs in DIO, however, are unknown. We tested the hypothesis that overactive parasympathetic signaling at muscarinic acetylcholine receptors (mAChRs) in the SI increases biosynthesis of the eCB, 2-arachidonoyl-*sn*-glycerol (2-AG), which drives hyperphagia via local CB_1Rs in DIO. Male mice were maintained on a high-fat/high-sucrose western-style diet for 60 days, then administered several mAChR antagonists 30 min prior tissue harvest or a food intake test. Levels of 2-AG and activity of its metabolic enzymes in the SI were quantitated. DIO mice, when compared to those fed a low-fat/no-sucrose diet, displayed increased expression of cFos protein in the dorsal motor nucleus of the vagus, which suggests increased activity of efferent cholinergic neurotransmission. These mice exhibited elevated levels of 2-AG biosynthesis in the SI, which was reduced to control levels by mAChR antagonists. Moreover, the peripherally-restricted mAChR antagonist, methylhomatropine bromide, and the peripherally-restricted CB_1R antagonist, AM6545, reduced food intake in DIO mice for up to 24 h but had no effect in mice conditionally deficient in SI CB_1Rs. These results suggest that hyperactivity at mAChRs in the periphery increases formation of 2-AG in the SI and activates local CB_1Rs, which drives hyperphagia in DIO.

Significance Statement

Gut-brain signaling controls food intake and energy homeostasis; however, it is poorly understood how gut-brain signaling becomes dysregulated in obesity. In this study, we demonstrated that brain to gut communication is altered in obesity, leading to an increase in endocannabinoid signaling in the GI tract, which drives overeating. Acutely blocking activity at muscarinic acetylcholine receptors in the periphery attenuates intestinal endocannabinoid production and calorie intake in obese animals. This effect was absent in mice conditionally lacking CB_1Rs in the intestinal epithelium. These findings expand our understanding of the complex pathophysiology associated with obesity and mechanisms of brain-gut-brain signaling.

Introduction

Food intake and energy balance are controlled by gut-brain neurotransmission, and this communication becomes dysregulated in obesity (Berthoud, 2008; de Lartigue et al., 2011; de Lartigue et al., 2014; Argueta et al., 2019; McDougle et al., 2021). For example, vagal afferent neurons in diet-induced obese (DIO) mice displayed impaired responses to the satiation peptide, cholecystokinin (CCK) (Daly et al., 2011), as well as reduced sensitivity to mechanical stimulation (Kentish et al., 2012) and leptin signaling (de Lartigue et al., 2011). Mounting evidence also suggests that overactive endocannabinoid (eCB) signaling in the upper small-intestinal lining in DIO mice (Artmann et al., 2008; Izzo et al., 2009; Argueta and DiPatrizio, 2017) contributes to overeating and dysregulated gut brain-mediated satiation by a mechanism that includes inhibiting nutrient-induced CCK release (Argueta et al., 2019; DiPatrizio, 2021). Furthermore, recent studies highlight an important function for gut-brain communication in the control of food preferences and reward (Han et al., 2018; Sclafani, 2018; Li et al.,

2022), and the contribution of gut-brain eCB signaling in these processes (DiPatrizio et al., 2013; Avalos et al., 2020; Berland et al., 2022). Indeed, acute preferences for western-style high-fat/sucrose diets versus low-fat/no-sucrose diets are absent in mice conditionally lacking cannabinoid subtype-1 receptors (CB_1Rs) in intestinal epithelial cells, which underscores an essential role for CB_1Rs in the intestinal lining in gut-brain control of preferences for palatable foods (Avalos et al., 2020).

Less is known about how obesity affects activity of vagal efferent neurons, which provide dense cholinergic innervation to the gastrointestinal tract from the caudal brainstem (Berthoud et al., 1991; Altschuler et al., 1993). Nonetheless, early studies suggest that this parasympathetic neurotransmission may play an important role in brain-gut signaling that controls feeding behavior. The peripherally-restricted muscarinic acetylcholine receptor (mAChR) antagonist, atropine methyl nitrate, inhibited intake of a liquid diet in sham-feeding rats (Lorenz et al., 1978) and prevented refeeding after a fast (Pradhan and Roth, 1968). In addition, activity of cholinergic efferent vagal neurons that project from the dorsal motor nucleus of the vagus (DMV) to the gut is controlled by central melanocortin-4 receptors (MC4Rs) (Sohn et al., 2013), which play a key role in energy homeostasis and attenuation of food intake (Williams and Elmquist, 2012). Specific roles for the eCB system in brain-gut cholinergic control of food intake and its dysregulation in obesity, however, are unclear.

Several reports suggest that mAChR signaling controls eCB production in the central nervous system (Kim et al., 2002; Straiker and Mackie, 2007; Zhao and Tzounopoulos, 2011; Rinaldo and Hansel, 2013). Similarly, cholinergic signaling in the periphery stimulates biosynthesis of orexigenic eCBs in the upper small-intestinal epithelium of fasted rats, an effect that was blunted by surgical resection of the vagus nerve below the diaphragm or after administration of several mAChR antagonists (DiPatrizio et al., 2015). Moreover, tasting dietary fats increased biosynthesis of eCBs in this organ and promoted further intake of fat through activating local CB_1Rs (DiPatrizio et al., 2011; DiPatrizio et al., 2013). This increased eCB activity was also blocked in vagotomized animals. Together, these studies suggest an

important role for the efferent vagus nerve in the biosynthesis of appetite-promoting eCBs in cells lining the upper intestine.

A primary biosynthetic pathway for the abundant eCB, 2-arachidonoyl-*sn*-glycerol (2-AG), requires a two-step enzymatic process that includes phospholipase C (PLC) and diacylglycerol lipase (DGL) activity (Stella et al., 1997; Piomelli et al., 2007; Aaltonen et al., 2014). This pathway can be activated by metabotropic receptors coupled to G_q-type g-proteins such as group I metabotropic glutamate receptors or muscarinic acetylcholine receptor sub-types 1 and 3 (M_1 and M_3, respectively) (Hulme et al., 1990; Caulfield and Birdsall, 1998; Jung et al., 2007; Aaltonen et al., 2014). Here, we tested the hypothesis that overactive parasympathetic signaling at mAChRs increases biosynthesis of 2-AG in the upper small-intestinal epithelium in DIO, which drives overeating via local CB_1Rs.

Materials & Methods

Animals

C57BL/6 male mice (Taconic, Oxnard, CA, USA) or transgenic mice (described below in *Transgenic Mouse Generation*) 8-10 weeks of age were group-housed with *ad-libitum* access to standard rodent laboratory diet (SD; Teklad 2020x, Envigo, Huntingdon, UK; 16% kcal from fat, 24% kcal from protein, 60% kcal from carbohydrates) or Western Diet (WD; Research Diets D12709B, New Brunswick, NJ, USA; 40% kcal from fat, 17% kcal from protein, 43% kcal from carbohydrates as mostly sucrose) and water throughout all experiments unless otherwise stated. Mice were maintained on a 12-h dark/light cycle beginning at 1800 h. All procedures met the U.S. National Institute of Health guidelines for care and use of laboratory animals and were approved by the Institutional Animal Care and Use Committee (IACUC) of the University of California, Riverside.

Transgenic Mouse Generation

Conditional intestinal epithelium-specific CB_1R-deficient mice (IntCB_1-/-, Cnr1$^{tm1.1\ mrl}$/vil-cre ERT2) were generated by crossing Cnr1-floxed mice (IntCB_1+/+, Cnr1$^{tm1.1\ mrl}$; Taconic, Oxnard, CA, USA; Model #7599) with Vil-CRE ERT2 mice donated by Dr. Randy Seeley (University of Michigan, Ann Arbor, MI, USA) with permission from Dr. Sylvie Robin (Curie Institute, Paris, France). Cre recombinase expression in the intestinal epithelium is driven by the villin promotor, which allows for conditional tamoxifen-dependent Cre recombinase action to remove the *Cnr1* gene from these cells, as described by el Marjou et al. (el Marjou et al., 2004). Cnr1$^{tm1.1\ mrl}$/vil-cre ERT2 mice used in these experiments are referred to as IntCB_1-/-, and Cnr1$^{tm1.1\ mrl}$ control mice (lacking Cre recombinase) are referred to as IntCB_1+/+. Tail snips were collected from pups at weaning and DNA was extracted and analyzed by conventional PCR using the following primers (5'-3'): GCAGGGATTATGTCCCTAGC (CNR1-ALT), CTGTTACCAGGAGTCTTAGC (1415-35), GGCTCAAGGAATACACTTATACC (1415-37), GAACCTGATGGACATGTTCAGG (vilcre, AA), AGTGCGTTCGAACGCTAGAGCCTGT (vilcre, SS), TTACGTCCATCGTGG-ACAGC (vilcre, MYO F), TGGGCTGGGTGTTAGCCTTA (vilcre, MYO R). Knockdown of Cnr1 expression in the intestinal epithelium was verified by RT-qPCR immediately following feeding behavior experiments (intCB_1+/+ control mice, 1.000 ± 0.2869; intCB_1-/- mice, 0.1226 ± 0.0149; $t_{(13)} = 3.282$, $p = 0.0060$ via two-tailed t-test).

Drug Preparation and Administration

IntCB_1-/- and intCB_1+/+ mice were administered tamoxifen (IP, 40 mg per kg) daily for five consecutive days. Tamoxifen (Sigma-Aldrich, St. Louis, MO, USA) was dissolved in corn oil using bath sonication at a concentration of 10 mg per mL then stored at 37°C protected from light until administration. Mice were group housed in disposable cages (14.7 x 9.2 x 5.5") at up to 5 mice per cage throughout the injection period and for a 3-day post-injection period. JZL-184 (Tocris, Bristol, UK) was incubated with intestinal epithelium tissue homogenate to inhibit MGL activity in the DGL enzyme

activity assay. The peripherally-restricted non-selective muscarinic acetylcholine receptor antagonist methylhomatropine (bromide) (ATR; Cayman Chemicals, Ann Arbor, MI, USA) was dissolved in 0.9% sterile sodium chloride solution (LabChem, Zelienople, PA, USA) and administered (IP, 2 mg per kg per 2 mL) 30 minutes prior to tissue harvest and testing. The selective muscarinic M_3 receptor antagonist DAU 5884 hydrochloride (DAU; Tocris Bioscience, Minneapolis, MN, USA) was dissolved in 0.9% sterile sodium chloride solution (LabChem, Zelienople, PA, USA) and administered (IP, 2 mg per kg per 2 mL) 30 minutes prior to tissue harvest and testing. The selective muscarinic M_1 receptor antagonist Pirenzepine dihydrochloride (PIR; Sigma-Aldrich, St. Louis, MO, USA) was dissolved in 0.9% sterile sodium chloride solution (LabChem, Zelienople, PA, USA) and administered (IP, 2 mg per kg per 2 mL) 30 minutes prior to tissue harvest and testing. The peripherally-restricted CB_1R neutral antagonist AM6545 (Northeastern University Center for Drug Discovery, Boston, MA, USA) was administered (IP, 10 mg per kg per 2 mL) 30 minutes prior to testing. All antagonists were administered 30 minutes prior to testing to match conditions of our previously published experiments (Argueta and DiPatrizio, 2017; Avalos et al., 2020). The vehicle for AM6545 consisted of 7.5% dimethyl sulfoxide (DMSO, Sigma-Aldrich, St. Louis, MO, USA), 7.5% Tween 80 (Chem Implex Intl Inc., Wood Dale, IL, USA), and 85% 0.9% sterile sodium chloride solution (LabChem, Zelienople, PA, USA).

Lipid Extraction

Animals were anesthetized with isoflurane at the time of tissue harvest (0900 h) following *ad libitum* food and water access. Jejunum was quickly removed and washed in ice cold phosphate-buffered saline (PBS), opened longitudinally on a stainless-steel tray on ice, and contents were removed. Jejunum mucosa was isolated using glass slides to scrape epithelial layer and was snap-frozen in liquid nitrogen (N_2). Samples were stored at -80°C until analysis. Frozen tissues were weighed and then homogenized in 1 mL methanol (MeOH) solution containing 500 pmol [$^2H_5$]-2-AG, 5 pmol [$^2H_4$]-AEA, and 5 pmol [$^2H_4$]-OEA or 500 pmol of dinonadecadienoin (19:2 diacylglycerol, 19:2 DAG; Nu-Check Prep,

Waterville, MN, USA) as internal standards. Lipids were extracted as previously described (Argueta and DiPatrizio, 2017) and resuspended in 0.2 mL $CHCl_3$:MeOH (1:1). 1 µL of the resulting sample was analyzed via ultra-performance liquid chromatography/tandem mass spectrometry (UPLC-MS/MS).

LCMS Detection of 1-stearoyl, 2-arachidonoyl-sn-lycerol (SAG) and MAGs

Data were acquired using an Acquity I Class UPLC with direct connection to a Xevo TQ-S Micro Mass Spectrometer (Waters Corporation, Milford, MA, USA) with electrospray ionization (ESI) sample delivery. 2-Arachidonoyl-*sn*-Glycerol (2-AG) and other analytes were detected as previously described (Argueta et al., 2019). SAG was separated using an Acquity UPLC BEH C_{18} column (2.1 mm x 50 mm i.d., 1.7 µm, Waters Corporation), and eluted by a gradient of water, isopropyl alcohol (IPA), and acetonitrile (ACN) containing 10 mM NH_4 formate at a flow rate of 0.4 mL per min and gradient: 80% ACN:water (60:40) and 20% ACN:IPA (10:90) 0.5 min, 80% to 0% ACN:water 0.5 – 6.0 min, 0% ACN:water 6.0 – 6.25 min, 0% to 80% ACN:water 6.25 – 6.50 min. The column was maintained at 50°C, and samples were kept at 10°C in accompanying sample manager. MS/MS detection was in positive ion mode with capillary voltage maintained at 1.10 kV, and argon (99.998%) was used as collision gas. Cone voltages and collision energies for respective analytes: SAG (18:0, 20:4) = 38v, 14v; 2-AG (20:4) = 30v, 12v; 2-OG (18:1) = 42v, 10v; 2-DG (22:6) = 34v, 14v; 2-LG (18:2) = 30v, 10v; 19:2 DAG = 26v, 14v; [$^2H_5$]-2-AG = 25v, 44v. Lipids were quantitated using a stable isotope dilution method detecting H^+ or Na^+ adducts of the molecular ions $[M + H/Na]^+$ in multiple reaction monitoring mode (MRM). Extracted ion chromatograms for MRM transitions were used to quantitate analytes: SAG (*m/z* = 662.9> 341.3), 2-AG (*m/z* = 379.3 > 287.3), 2-OG (*m/z* = 357.4 > 265.2), 2-DG (*m/z* = 403.3 > 311.2), 2-LG (*m/z* = 355.3 > 263.3), with 19:2 DAG (*m/z* = 662.9 > 627.5) as internal standard for SAG, and [$^2H_5$]-2-AG (*m/z* = 384.3 > 93.4) as internal standard for all MAGs. One “blank” sample that did not include any experimental tissue was processed and analyzed in the same manner as all other samples. This control revealed no detectable eCBs and related lipids included in our analysis.

Enzyme Activity Assays

Intestinal epithelium was collected as described above (*Lipid Extracts*) and approximately 100 mg of frozen tissue was homogenized in 2 mL of ice-cold 50 mM Tris-HCl, 320 mM sucrose (pH 7.5) buffer, as previously described (Wiley et al., 2021). Homogenates were centrifuged at 800 g for 10 min at 4°C and supernatant was collected. Protein supernatants were sonicated twice for 10 s and then freeze-thawed in liquid N_2 twice. Samples were spun again, and supernatant protein content was quantified using BCA assay and diluted to working concentration with Tris-HCl/sucrose buffer. For the DGL activity assay, small-intestinal epithelial tissue homogenates (25 µg, room temperature) were incubated with the MGL inhibitor, JZL-184 (0.3 µM; Tocris, Bristol, UK), and any other drugs tested for 10 minutes. Homogenates were then incubated in 0.2 mL Tris-HCl with 0.2% Triton X-100 (pH 7.0 at 37°C) containing 20 nmol 19:2 DAG (Nu-Check Prep, Waterville, MN, USA) at 37°C for 30 min. Reactions were stopped by adding 1 mL ice-cold methanol containing 25 pmol [$^2H_5$]-2-AG as internal standard. Lipids were extracted and the product of the reaction, mononononadecadienoin (19:2 monoacylglycerol, 19:2 MAG), was analyzed via UPLC-MS/MS as previously described (Argueta et al., 2019). For the MGL activity assay, small-intestinal epithelial tissue (10 µg) was incubated with 0.4 mL Tris-HCl with 0.1% bovine serum albumin (BSA) (pH 8.0 at 37°C) containing 50 nmol 19:2 MAG (Nu-Check Prep, Waterville, MN, USA; final volume 0.5 mL per reaction) at 37°C for 10 min. Reactions were stopped by adding 1 mL MeOH containing 10 nmol heptadecanoic acid (17:1 free fatty acid, 17:1 FFA; Nu-Check Prep) as internal standard. Lipids were extracted and the product of the reaction (19:2 free fatty acid, 19:2 FFA) was analyzed via UPLC-MS/MS as previously described (Argueta et al., 2019). GraphPad Prism software generated the following error message for the enzyme inhibition curves in **Figures 6*B*, *C*,** and ***D***: *"For at least one parameter, Prism was able to find a best-fit value but was unable to calculate a complete confidence interval. This best-fit value should be interpreted with caution".* Negative R^2 values are

indicative of no correlation between the drug concentration and enzyme activity, so we included this information to further demonstrate that DAU, PIR, and ATR are not directly inhibiting DGL activity.

Feeding Behavior

Mice were single-housed in two-hopper feeding chambers (TSE Systems, Chesterfield, MO, USA) for five days to acclimate, and received *ad-libitum* access to food and water throughout behavioral testing. Total caloric intake of each diet (kcal), water intake (mL), and distance travelled (km) were calculated every minute across the testing period, beginning at the start of the dark cycle (1800 h) for 24 h. Data were processed using TSE Phenomaster software, as previously described (Avalos et al., 2020).

Gene Expression

Total RNA from intestinal epithelium tissue was extracted using an RNeasy kit (Qiagen, Valencia, CA, USA) and first-strand cDNA was generated using M-MLV reverse transcriptase (Invitrogen, Carlsbad, CA, USA). Areas used for tissue collection and processing were sanitized with 70% ethanol solution then treated with RNAse inhibitor (RNAse Out, G-Biosciences, St. Louis, MO, USA). Reverse transcription of total RNA was performed as previously described (Argueta et al., 2019). Quantitative RT-PCR was performed using preconfigured SYBR green PrimePCR assays (Biorad, Irvine, CA, USA) with the primer for the CB_1R (Cnr1) gene transcript. Hprt was used as a housekeeping gene. Reactions were run in duplicates and values expressed as relative mRNA expression.

cFos Immunohistochemistry

On the day of the experiment, mice were allowed *ad-libitum* access to food and water for the entire day, and then fasted 30 minutes prior to the onset of the dark cycle (1730h) to reduce gut-brain feedback resulting from food consumption. cFos protein can be detected 20-90 minutes following the stimulus (Bullitt, 1990), therefore mice were perfused between 1845h and 1915h (45-75 minutes

following the onset of the dark period) to enable optimal cFos detection in the brainstem. Experiments occurred in the absence of any drug or other treatment to examine whether DMV neuronal activation differs between SD- and WD-fed mice in basal conditions. Animals were deeply anesthetized with isoflurane and transcardially perfused with 40 mL of ice-cold PBS immediately followed by 40 mL of ice-cold 4% paraformaldehyde (PFA). The brainstem was immediately collected and stored at 4°C overnight in 4% PFA. Brainstems were transferred to a solution containing 30% sucrose and 0.01% sodium azide in PBS and stored at 4°C until adequate cryopreservation was achieved (when tissue had completely sunk to the bottom of the solution). Brainstems were stored in OCT compound at -20°C until processing. On the day of the assay, 50 µM sections of the medulla were transferred to PBS and then sequentially incubated (including PBS and/or PBST wash steps between incubations) in: 1) 10 mM citrate buffer, pH 6.0; 2) 4% normal goat serum (NGS) (Millipore Sigma, Burlington, MA, USA) in PBST; 3) anti-cFos rabbit monoclonal antibody (1:500, Cell Signaling Technology, Danvers, MA, USA) or anti-ChAT monoclonal antibody (1:500, Invitrogen, Carlsbad, CA, USA) in blocking buffer; 4) anti-rabbit IgG Alexa Fluor 488 conjugate (1:500, Cell Signaling Technology, Danvers, MA, USA) or donkey anti-IgG (H+L) Alexa Fluor 555 (1:500, Invitrogen, Carlsbad, CA, USA) in blocking buffer. Sections were mounted on glass slides, allowed to air-dry overnight, and coverslips were added with VECTASHIELD mounting medium with DAPI (Vector Laboratories, Newark, CA, USA) prior to imaging.

Microscopy & Image Analysis

Fluorescent images were taken on a Zeiss 200 M fluorescence deconvolution microscope equipped with a computer-controlled stage and the appropriate filters for DAPI and FITC (Carl Zeiss Microscopy GmbH, Jena, Germany). Slidebook software (version 6, Intelligent Imaging Innovations, Inc., Denver, CO) was used for all image acquisition. Quantitative analysis of $cFos^+$ and $ChAT^+$ cells in the DMV was performed as described previously (Igelstrom et al., 2010; Perrin-Terrin et al., 2016). Briefly, one section per animal was imaged at 10× so that local landmarks were visible to enable consistent analysis

between samples. The exposure period was kept the same for all analyzed images. Immunoreactivity was quantified using Fiji open-source software (Schindelin et al., 2012). Images were subject to identical black/white thresholding to enable counting of positive nuclei. Immunoreactive puncta were counted using the Particle Analysis function within bilateral fixed areas of each image.

Experimental Design & Statistical Analysis

Details regarding the experimental design of individual experiments are provided in the figure legends. Data were analyzed by GraphPad Prism version 9.5.0 (GraphPad Software, La Jolla, CA, USA) using unpaired Student's *t*-tests (two-tailed), one-way ANOVA, two-way ANOVA, or three-way ANOVA with Holm-Sidak's multiple comparisons *post-hoc* test when appropriate. Inhibition curves in **Figure 6** were generated using a least squares fit of log[inhibitor] vs. normalized response. Results are expressed as means ± S.E.M. and significance was determined at $p<0.05$.

Results

Neuronal activity is increased in the DMV of DIO animals

We tested the hypothesis that parasympathetic neurotransmission is overactive in DIO, which drives overproduction of gut eCBs and associated hyperphagia. $cFos^+$ cells in the dorsal motor nucleus of the vagus (DMV) of untreated lean control mice fed SD (**Fig. 1*A***) and DIO mice fed WD (**Fig. 1*B***) were quantified. WD-fed mice exhibited an increased number of $cFos^+$ cells in the DMV when compared to SD-fed controls, which suggests increased activity of DMV neurons in obesity (**Fig. 1*C***). To confirm that the hyperactive cells within the DMV of the mice fed WD were cholinergic, we quantified immunoreactivity for cFos and choline acetyltransferase (ChAT, the biosynthetic enzyme for acetylcholine) in the DMV in a second cohort of mice fed SD or WD. 73.73% of the $cFos^+$ cells in the DMV of mice fed WD were also

immunoreactive for ChAT indicating that most hyperactive cells in the DMV are indeed cholinergic (**Fig.1*D, G***). These mice not only exhibited an increased number of $cFos^+$ cells in the DMV (**Fig. 1*E***), but also an increased number of $cFos^+$ and $ChAT^+$ dual-labeled cells in the DMV when compared mice fed SD (**Fig. 1*F***). Mice fed WD, when compared to those maintained on SD, also gained significantly more body weight (**Fig. 2*A***), demonstrated increased change in body weight (**Fig. 2*B***), consumed more calories (**Fig. 2*C***), and displayed increased epididymal fat mass (**Fig. 2*D***), similar to previous studies (Argueta and DiPatrizio, 2017; Argueta et al., 2019).

mAChR antagonism normalizes eCB levels in the upper intestinal epithelium in DIO mice

We next investigated whether pharmacological inhibition of mAChRs can block overactive eCB production in the upper small-intestinal epithelium. Consistent with our previous findings (Argueta and DiPatrizio, 2017; Argueta et al., 2019), mice fed WD exhibited higher levels of 2-AG in the upper small-intestinal epithelium (**Fig. 3*A***) when compared to SD control mice. WD mice treated with a single IP injection of the selective M_3 mAChR antagonist, DAU (2 mg per kg), had significantly reduced levels of 2-AG (**Fig. 3*A***) and other monoacylglycerols (**Fig. 3*B, C***) in the upper small-intestinal epithelium when compared to vehicle-treated mice fed WD. Notably, levels were reduced to those found in SD mice. Treatment with the selective M_1 mAChR antagonist, PIR (2 mg per kg), reduced levels of 2-AG in WD mice when compared to vehicle; however, this effect was not significant for 2-AG (**Fig**. **3*A***) but was significant for select other MAGs (**Fig. 3C**). Given this result, we performed a dose-response analysis to examine the effects of several doses of PIR within a log step of 2 mg per kg on MAG levels in the small-intestinal epithelium of WD-fed mice (**Fig. 4*A-D***, doses of 0.0, 0.65, 2.0, and 6.5 mg per kg). PIR at 2.0 mg per kg, but not 0.65 or 6.5 mg per kg, significantly reduced levels of 2-AG (**Fig. 4*A***) and select other MAGs (**Fig. 4*B***) in the small-intestinal epithelium. Lastly, the peripherally-restricted non-selective mAChR

antagonist, ATR (2 mg per kg), reduced levels of 2-AG (**Fig. 3*A***) and select other MAGs (**Fig. 3*B***) in mice fed WD to levels found in mice fed SD.

SAG formation and DGL activity in jejunum mucosa are inhibited by mAChR antagonism

We next tested if changes in metabolism of monoacylglycerols (see **Fig. 5*D***) in the upper small-intestinal epithelium led to increased levels of 2-AG in WD mice and the ability for mAChR antagonists to normalize levels to those found in SD control mice. We first analyzed levels of the diacylglycerol precursor of 2-AG, 1-stearoyl,2-arachidonoyl-*sn*-glycerol (SAG). Like 2-AG, levels of SAG were significantly elevated in the intestinal epithelium of vehicle-treated WD mice when compared to vehicle-treated SD mice, and treatment with DAU (2 mg per kg), PIR (2 mg per kg), and ATR (2 mg per kg) reduced SAG levels in WD mice to those found in SD mice (**Fig. 5*A***). Furthermore, activity of diacylglycerol lipase (DGL) – an eCB biosynthetic enzyme responsible for the hydrolysis of SAG and its conversion to 2-AG – was similarly reduced by treatment with mAChR antagonists (**Fig. 5*B***). Activity of monoacylglycerol lipase (MGL), a primary degradative enzyme responsible for 2-AG inactivation (Dinh et al., 2002) was not significantly affected by drug treatments (**Fig. 5*C***).

Anticholinergics do not affect 2-AG metabolic enzyme activity ex vivo

We utilized our UPLC/MS^2-based DGL activity assay (Wiley et al., 2021) to confirm that DGL activity was not directly disrupted *ex vivo* by any of the drugs used *in vivo*. Activity of DGL in intestinal epithelium tissue from WD mice was inhibited in a concentration-dependent manner by an inhibitor of DGL, tetrahydrolipstatin (THL, 3nM to 1μM range) (**Fig. 6*A***). In contrast to THL, incubation of tissue with a wide range of concentrations of mAChR antagonists used in these studies including ATR (**Fig. 6*B,*** 10nM

to 10μM range), DAU (**Fig. 6*C,*** 10nM to 100μM range), and PIR (**Fig. 6*D,*** 10nM to 10μM range) failed to affect enzymatic activity of DGL, which suggests that these drugs do not directly interfere with DGL activity.

mAChR antagonism reduces caloric intake in DIO mice

Roles for peripheral mAChRs and CB_1Rs in overeating were evaluated next in mice fed WD. A single dose of ATR (2mg per kg) reduced caloric intake for up to 24 h in WD mice (**Fig. 7*A***) but had no effect in SD mice (**Fig. 7*B***). Moreover, ATR treatment in WD mice reduced caloric intake to similar levels induced by the peripherally-restricted CB_1R antagonist, AM6545 (**Fig. 7*A*,** 10 mg/kg). When ATR and AM6545 were co-administered in WD mice, caloric intake was comparable to intakes found after administration of each drug alone (**Fig. 7*A***). Treatment with AM6545 alone or in combination with ATR did not significantly affect intake in SD mice (**Fig. 7*B***). A single injection of DAU (2mg per kg) also caused a reduction in caloric intake in WD mice – but not SD mice – for up to 12 h (**Fig. 7*C*, 7*D***). In contrast to DAU and ATR, PIR (2mg per kg) had no effect on intake irrespective of diet (**Fig. 7*E*, 7*F***). ATR and AM6545 each had a minor effect on ambulation in mice fed WD (**Fig. 8*A***), while ATR and AM65645 in combination reduced ambulation in both mice fed WD and in lean mice (**Fig. 8*A, 8C***, respectively, and accompanying **Table 1**). DAU did not impact ambulation but did have an overall effect on water intake in WD mice (**Fig. 8*E*, 8*F,* respectively,** and accompanying **Table 1**), which may be a result of reduced food intake (**Fig. 7*C***). PIR at 2 mg per kg had no effect on water intake or ambulation in WD or SD mice (**Fig. 8*I,* 8*J*, 8*K*, 8*L*).**

Based on our findings from the biochemical dose response analysis of PIR (**Fig. 4*A*-*D***), we aimed to examine the effects of the same doses of PIR on food intake, water intake, and ambulation. PIR did not significantly affect water intake (**Fig. 4*F***) or ambulation (**Fig. 4*G***) in WD-fed animals at any of the

doses tested (0.0, 0.65, 2.0, 6.5 mg per kg). A mild main effect of dose on food intake was observed (**Fig. 4*E***, p=0.02 for dose by 2-way ANOVA); however, no significant differences were detected between doses in a *post-hoc* multiple comparisons analysis.

Inhibiting peripheral CB_1Rs or mAChRs failed to affect food intake in mice conditionally lacking CB_1Rs in the intestinal epithelium

We next utilized conditional intestinal epithelium-specific CB_1R-deficient mice [intCB_1-/- (Avalos et al., 2020; Wiley and DiPatrizio, 2022)] to determine if CB_1Rs in intestinal epithelial cells were required for the appetite-suppressing effects of peripherally-restricted CB_1R and mAChR antagonists in obese WD mice. IntCB_1-/- mice and control mice with functional CB_1Rs in the intestinal epithelium (intCB_1+/+) were placed on WD for 60 days. AM6545 (10 mg/kg) or ATR (2 mg/kg) treatment reduced caloric intake for up to 24 hours in WD intCB_1+/+ control mice (**Fig. 9*A***). Notably, however, neither drug had an effect on intake in WD intCB_1-/- mice (**Fig. 9*B***). Both intCB_1+/+ and intCB_1-/- mice had largely similar body weights throughout diet exposure (**Fig. 9*C***); however, analysis of change in body weight from baseline by two-way ANOVA revealed a genotype effect that indicated intCB_1-/- mice had lower body weight gain when compared to intCB_1+/+ control mice (**Fig. 9*D***). Independently, AM6545 reduced ambulation in intCB_1+/+ mice, but had no effect on ambulation in intCB_1-/- animals (**Fig. *10A, C*** and **Table 2**). ATR also yielded a minor effect on ambulation in IntCB_1+/+ mice (**Fig. 10*A***). AM6545 reduced water intake in intCB_1-/- mice but did not affect water intake in intCB_1+/+ mice (**Fig. 10*B, D*** and accompanying **Table 2**).

Discussion

We report that *(i)* cholinergic neuronal activity in the DMV of DIO mice is increased when compared lean mice, *(ii)* cholinergic activity at peripheral mAChRs in DIO promotes biosynthesis of 2-AG in the upper-intestinal epithelium by a mechanism that includes increased production of local 2-AG precursors and their conversion to 2-AG, and *(iii)* CB_1Rs in the intestinal epithelium are required for hyperphagia associated with overstimulation of these pathways in DIO. These results suggest a novel brain-gut mechanism that drives overeating in DIO through interactions between cholinergic neurotransmission and orexigenic eCB signaling in the gut.

DIO mice, when compared to lean controls, displayed a significantly larger number of $cFos^+$ and dual-labeled $cFos^+$ $ChAT^+$ cells in the DMV, which suggests increased activity of efferent parasympathetic vagal fibers. The DMV is the primary source of parasympathetic input to the digestive system (Gibbons, 2019); indeed, over 70% of the cFos+ cells in the DMV of the WD-fed mice were shown to be immunoreactive for ChAT. Though it is likely that these overactive cholinergic cells in the DMV are the source of increased parasympathetic activity in the GI tract of the obese mice, motor neurons originating in the DMV have functionally and anatomically discrete outputs to distinct segments of the gastrointestinal tract and other organs (Rogers et al., 2006; Schubert and Peura, 2008; Mawe et al., 2018; Tao et al., 2021). Future experiments will be necessary to further confirm if the same DMV neurons that are activated in obese mice are the source of mAChR hyperactivity that leads to overproduction of 2-AG in the upper small-intestinal epithelium.

Although not quantified, an increase in the number of $cFos^+$ cells in other regions of the intermediate medulla, namely the nucleus of the solitary tract (NTS), were observed. Thus, it is possible that a general dysregulation within the medulla of obese mice occurs. Accordingly, it was recently reported that the daily rhythms of oscillating cells within the NTS are disrupted by exposure to high-fat diet (Chrobok et al., 2022b). The same group also demonstrated that high-fat diet exposure amplified the daily variation of time-keeping cells within the DMV and blunted neuronal responsiveness to

metabolic neuromodulators (Chrobok et al., 2022a). These studies and others (Kentish et al., 2012; Kentish et al., 2016; Clyburn et al., 2018; Zhang et al., 2020; Kovacs and Hajnal, 2022) support the notion that select brainstem nuclei, which are responsible for sensing nutritional status and maintaining metabolic homeostasis (i.e., DMV and NTS), become dysregulated in response to metabolic challenges.

Our data reveal a key role for peripheral mAChRs in controlling eCB biosynthesis in the intestinal epithelium in DIO mice. These animals had elevated levels of *(i)* the 2-AG precursor, SAG, *(ii)* activity of the biosynthetic enzyme for 2-AG and other MAGs, DGL, and *(iii)* 2-AG in the intestinal epithelium, which was all attenuated by treatment with the M_3-selective antagonist, DAU, or the non-selective peripherally-restricted mAChR antagonist, ATR. Moreover, the M_1-selective antagonist, PIR, was effective at reducing both SAG and DGL activity levels; however, it only significantly reduced 2-AG levels in the follow-up dose response experiment at the 2.0 mg per kg dose, but not 0.65 or 6.5 mg per kg (**Fig.4*A***). It is notable that while M_1 antagonism did influence MAG formation within the intestinal epithelium, it did not significantly affect feeding behavior at any dose tested. Together, these results suggest a more prominent role for the M_3 mAChR subtype in driving eCB biosynthesis and overeating in DIO, and also highlight the necessity for future experiments exploring roles for M_1 versus M_3 mAChRs in food intake and related behaviors. Furthermore, we reported that following 24 hr of food deprivation (another metabolic challenge that has been shown to elevate intestinal 2-AG), DAU – but not PIR – blocked biosynthesis of 2-AG in the upper small-intestinal epithelium of rats (DiPatrizio et al., 2015). In addition, M_3 mAChR activation in the central nervous system initiates a signaling cascade that rapidly upregulates expression of Cnr1 mRNA and potentiates responses to CB_1R agonists, such as 2-AG (Marini et al., 2023). Given that mRNA for both M_1 and M_3 subtypes is expressed in mouse duodenum, jejunum, and ileum epithelial cells (Muise et al., 2017), future studies should determine the expression patterns of these receptors in specific cell types and their co-localization with eCB metabolic enzymes and CB_1Rs throughout the gastrointestinal tract.

Our results suggest that pharmacological inhibition of peripheral M_3 mAChRs – alone or in combination with inhibitors of peripheral CB_1Rs – could be beneficial for reducing caloric intake in human obesity. This therapeutic strategy, however, may be met with deleterious side effects. For example, ATR alone or in combination with AM6545 led to reductions in ambulation (**Figures 8*A, C,* 10*A***). In addition, Cluny *et al*. reported that blocking peripheral CB_1Rs with daily injections of AM6545 did not cause malaise in rodents (Cluny et al., 2010); however, it is possible that ATR and AM6545 in combination may generate unfavorable effects. It should also be noted that M_3 mAChR antagonism may lead to a reduction in insulin secretion by pancreatic β-cells (Ruiz de Azua et al., 2011) and glucagon secretion by α-cells (Duttaroy et al., 2004), thereby suppressing the anorectic effect of these hormones and allowing feeding to return to baseline levels prematurely in the DAU-treated animals in our study (**Figure 7*C***). An additional concern associated with the therapeutic use of ATR is the role for M_2 mAChRs in the regulation of cardiac function (Peter et al., 2005). Cardiac function was not measured in the current study, but if ATR or related drugs are to be investigated for their potential as a treatment for obesity, possible cardiac side-effects must be considered.

The eCB system plays a critical role in the seeking and sensing of calorie-dense foods (DiPatrizio and Piomelli, 2012). Indeed, we reported a role for intestinal CB_1Rs in preferences for WD (Avalos et al., 2020). In these studies, mice treated with the CB_1R inverse agonist, AM251, displayed no preference for the highly palatable WD for up to 3 h. In addition, preferences for WD were largely abolished for up to 6 hours in mice conditionally lacking CB_1Rs in the intestinal epithelium. Notably, preferences for the WD returned by 24 h after initiation of the preference test in these mice. These findings suggest that *(i)* CB_1Rs in the intestinal epithelium are essential for acute preferences for high-fat, high-sugar foods and (*ii*) other biochemical mechanisms may override eCB control of food preferences over time and should be evaluated in the future (Avalos et al., 2020).

The eCB system also directly and indirectly interacts with afferent vagal signaling to control food intake, which becomes dysregulated in DIO (Argueta et al., 2019; Christie et al., 2020c; Christie et al., 2020a, b; DiPatrizio, 2021; Berland et al., 2022). For example, CB_1Rs are expressed in enteroendocrine I cells in the intestinal epithelium (Sykaras et al., 2012; Argueta et al., 2019). In response to nutrients entering the lumen, these cells produce and secrete the satiation peptide, CCK, which induces satiation via interactions with CCK_A receptors on afferent vagal fibers (Clemmensen et al., 2017). We reported that elevated levels of 2-AG in the small-intestinal epithelium of DIO mice inhibits gut-brain satiation signaling by a mechanism that includes blocking nutrient-induced release of CCK (Argueta et al., 2019). This effect was reversed by the peripheral CB_1R antagonist, AM6545, which restored the ability for nutrients to induce CCK release. Moreover, the hypophagic effects of AM6545 were completely reversed by a CCK_A antagonist in DIO mice. Together, these data suggest that in DIO, overactive eCB signaling at CB_1Rs on I cells in the upper-intestinal lining inhibits nutrient-induced CCK release, which may reduce activity of vagal afferent neurons and allow DIO mice to continue feeding past satiation. A direct test of this hypothesis, however, remains for future experiments. Future studies should also examine whether ATR treatment is reducing caloric intake in DIO mice via a similar CCK-mediated mechanism. While this work is yet to be completed, participation of the afferent vagus nerve in these processes is likely. Accordingly, multiple studies have revealed the necessity of intact vagal afferent signaling for preventing hyperphagia and weight gain, particularly in DIO (Covasa and Ritter, 1998; Daly et al., 2011; Kentish et al., 2012; de Lartigue et al., 2014; McDougle et al., 2021). In addition, recent studies identified a specialized subset of enteroendocrine cells lining the intestine that detect nutrients and communicate with vagal afferent fibers via functional synapses (Kaelberer et al., 2018; Kaelberer et al., 2020). Studies examining whether CB_1Rs also control neuropod activity in these processes and may become dysregulated in DIO remain to be performed.

In summary, our results identify a previously undescribed brain-gut pathway that recruits cholinergic signaling to drive eCB-mediated overeating in DIO. Components of this pathway may be targets for anti-obesity therapeutics.

References

Aaltonen N, Riera Ribas C, Lehtonen M, Savinainen JR, Laitinen JT (2014) Brain regional cannabinoid CB(1) receptor signalling and alternative enzymatic pathways for 2-arachidonoylglycerol generation in brain sections of diacylglycerol lipase deficient mice. Eur J Pharm Sci 51:87-95.

Altschuler S, Escardo J, Lynn R, Miselis R (1993) The Central Organization of the Vagus Nerve Innervating the Colon of the Rat. In, pp 502-509. Gastroenterology.

Argueta D, DiPatrizio N (2017) Peripheral endocannabinoid signaling controls hyperphagia in western diet-induced obesity. Physiology & Behavior 171:32-39.

Argueta D, Perez P, Makriyannis A, DiPatrizio N (2019) Cannabinoid CB1 Receptors Inhibit Gut-Brain Satiation Signaling in Diet-Induced Obesity. Frontiers in Physiology 10.

Artmann A, Petersen G, Hellgren LI, Boberg J, Skonberg C, Nellemann C, Hansen SH, Hansen HS (2008) Influence of dietary fatty acids on endocannabinoid and N-acylethanolamine levels in rat brain, liver and small intestine. Biochim Biophys Acta 1781:200-212.

Avalos B, Argueta D, Perez P, Wiley M, Wood C, DiPatrizio N (2020) Cannabinoid CB1 Receptors in the Intestinal Epithelium Are Required for Acute Western-Diet Preferences in Mice. Nutrients 12.

Berland C, Castel J, Terrasi R, Montalban E, Foppen E, Martin C, Muccioli GG, Luquet S, Gangarossa G (2022) Identification of an endocannabinoid gut-brain vagal mechanism controlling food reward and energy homeostasis. Mol Psychiatry 27:2340-2354.

Berthoud H, Carlson N, Powley T (1991) Topography of Efferent Vagal Innervation of the Rat Gastrointestinal-Tract. American Journal of Physiology 260:R200-R207.

Berthoud HR (2008) The vagus nerve, food intake and obesity. Regul Pept 149:15-25.

Bullitt E (1990) Expression of C-Fos-Like Protein as a Marker for Neuronal-Activity Following Noxious-Stimulation in the Rat. Journal of Comparative Neurology 296:517-530.

Caulfield MP, Birdsall NJ (1998) International Union of Pharmacology. XVII. Classification of muscarinic acetylcholine receptors. Pharmacol Rev 50:279-290.

Christie S, O'Rielly R, Li H, Wittert GA, Page AJ (2020a) Biphasic effects of methanandamide on murine gastric vagal afferent mechanosensitivity. The Journal of physiology 598:139-150.

Christie S, O'Rielly R, Li H, Wittert GA, Page AJ (2020b) High fat diet induced obesity alters endocannabinoid and ghrelin mediated regulation of components of the endocannabinoid system in nodose ganglia. Peptides 131:170371.

Christie S, O'Rielly R, Li H, Nunez-Salces M, Wittert GA, Page AJ (2020c) Modulatory effect of methanandamide on gastric vagal afferent satiety signals depends on nutritional status. The Journal of physiology 598:2169-2182.

Chrobok L, Klich JD, Jeczmien-Lazur JS, Pradel K, Palus-Chramiec K, Sanetra AM, Piggins HD, Lewandowski MH (2022a) Daily changes in neuronal activities of the dorsal motor nucleus of the vagus under standard and high-fat diet. J Physiol 600:733-749.

Chrobok L, Klich JD, Sanetra AM, Jeczmien-Lazur JS, Pradel K, Palus-Chramiec K, Kepczynski M, Piggins HD, Lewandowski MH (2022b) Rhythmic neuronal activities of the rat nucleus of the solitary

tract are impaired by high-fat diet - implications for daily control of satiety. J Physiol 600:751-767.
Clemmensen C, Muller TD, Woods SC, Berthoud HR, Seeley RJ, Tschop MH (2017) Gut-Brain Cross-Talk in Metabolic Control. Cell 168:758-774.
Cluny NL, Vemuri VK, Chambers AP, Limebeer CL, Bedard H, Wood JT, Lutz B, Zimmer A, Parker LA, Makriyannis A, Sharkey KA (2010) A novel peripherally restricted cannabinoid receptor antagonist, AM6545, reduces food intake and body weight, but does not cause malaise, in rodents. Br J Pharmacol 161:629-642.
Clyburn C, Travagli R, Browning K (2018) Acute high-fat diet upregulates glutamatergic signaling in the dorsal motor nucleus of the vagus. American Journal of Physiology-Gastrointestinal and Liver Physiology 314:G623-G634.
Covasa M, Ritter RC (1998) Rats maintained on high-fat diets exhibit reduced satiety in response to CCK and bombesin. Peptides 19:1407-1415.
Daly DM, Park SJ, Valinsky WC, Beyak MJ (2011) Impaired intestinal afferent nerve satiety signalling and vagal afferent excitability in diet induced obesity in the mouse. J Physiol 589:2857-2870.
de Lartigue G, Ronveaux CC, Raybould HE (2014) Deletion of leptin signaling in vagal afferent neurons results in hyperphagia and obesity. Mol Metab 3:595-607.
de Lartigue G, de la Serre C, Espero E, Lee J, Raybould H (2011) Diet-induced obesity leads to the development of leptin resistance in vagal afferent neurons. American Journal of Physiology-Endocrinology and Metabolism 301:E187-E195.
Dinh TP, Carpenter D, Leslie FM, Freund TF, Katona I, Sensi SL, Kathuria S, Piomelli D (2002) Brain monoglyceride lipase participating in endocannabinoid inactivation. Proceedings of the National Academy of Sciences of the United States of America 99:10819-10824.
DiPatrizio NV (2021) Endocannabinoids and the Gut-Brain Control of Food Intake and Obesity. Nutrients 13.
DiPatrizio NV, Piomelli D (2012) The thrifty lipids: endocannabinoids and the neural control of energy conservation. Trends Neurosci 35:403-411.
DiPatrizio NV, Joslin A, Jung KM, Piomelli D (2013) Endocannabinoid signaling in the gut mediates preference for dietary unsaturated fats. Faseb J 27:2513-2520.
DiPatrizio NV, Astarita G, Schwartz G, Li X, Piomelli D (2011) Endocannabinoid signal in the gut controls dietary fat intake. Proceedings of the National Academy of Sciences of the United States of America 108:12904-12908.
DiPatrizio NV, Igarashi M, Narayanaswami V, Murray C, Gancayco J, Russell A, Jung KM, Piomelli D (2015) Fasting stimulates 2-AG biosynthesis in the small intestine: role of cholinergic pathways. Am J Physiol Regul Integr Comp Physiol 309:R805-813.
Duttaroy A, Zimliki CL, Gautam D, Cui Y, Mears D, Wess J (2004) Muscarinic stimulation of pancreatic insulin and glucagon release is abolished in m3 muscarinic acetylcholine receptor-deficient mice. Diabetes 53:1714-1720.
el Marjou F, Janssen KP, Chang BH, Li M, Hindie V, Chan L, Louvard D, Chambon P, Metzger D, Robine S (2004) Tissue-specific and inducible Cre-mediated recombination in the gut epithelium. Genesis 39:186-193.
Gibbons CH (2019) Chapter 27 - Basics of autonomic nervous system function. In: Handbook of Clinical Neurology (Aminoff MJ, Boller F, Swaab DF, eds), pp 407-418: Elsevier.
Han W, Tellez LA, Perkins MH, Perez IO, Qu T, Ferreira J, Ferreira TL, Quinn D, Liu ZW, Gao XB, Kaelberer MM, Bohórquez DV, Shammah-Lagnado SJ, de Lartigue G, de Araujo IE (2018) A Neural Circuit for Gut-Induced Reward. Cell 175:887-888.
Hulme EC, Birdsall NJ, Buckley NJ (1990) Muscarinic receptor subtypes. Annu Rev Pharmacol Toxicol 30:633-673.

Igelstrom K, Herbison A, Hyland B (2010) ENHANCED c-Fos EXPRESSION IN SUPERIOR COLLICULUS, PARAVENTRICULAR THALAMUS AND SEPTUM DURING LEARNING OF CUE-REWARD ASSOCIATION. Neuroscience 168:706-714.

Izzo A, Piscitelli F, Capasso R, Aviello G, Romano B, Borrelli F, Petrosino S, Di Marzo V (2009) Peripheral endocannabinoid dysregulation in obesity: relation to intestinal motility and energy processing induced by food deprivation and re-feeding. British Journal of Pharmacology 158:451-461.

Jung KM, Astarita G, Zhu C, Wallace M, Mackie K, Piomelli D (2007) A key role for diacylglycerol lipase-alpha in metabotropic glutamate receptor-dependent endocannabinoid mobilization. Mol Pharmacol 72:612-621.

Kaelberer MM, Rupprecht LE, Liu WW, Weng P, Bohorquez DV (2020) Neuropod Cells: The Emerging Biology of Gut-Brain Sensory Transduction. Annual review of neuroscience 43:337-353.

Kaelberer MM, Buchanan KL, Klein ME, Barth BB, Montoya MM, Shen X, Bohorquez DV (2018) A gut-brain neural circuit for nutrient sensory transduction. Science 361.

Kentish S, Vincent A, Kennaway D, Wittert G, Page A (2016) High-Fat Diet-Induced Obesity Ablates Gastric Vagal Afferent Circadian Rhythms. Journal of Neuroscience 36:3199-3207.

Kentish S, Li H, Philp L, O'Donnell T, Isaacs N, Young R, Wittert G, Blackshaw L, Page A (2012) Diet-induced adaptation of vagal afferent function. Journal of Physiology-London 590:209-221.

Kim J, Isokawa M, Ledent C, Alger BE (2002) Activation of muscarinic acetylcholine receptors enhances the release of endogenous cannabinoids in the hippocampus. J Neurosci 22:10182-10191.

Kovacs P, Hajnal A (2022) Short-term high-fat diet consumption increases body weight and body adiposity and alters brain stem taste information processing in rats. Chemical Senses 47.

Li M, Tan HE, Lu Z, Tsang KS, Chung AJ, Zuker CS (2022) Gut-brain circuits for fat preference. Nature 610:722-730.

Lorenz D, Nardi P, Smith GP (1978) Atropine methyl nitrate inhibits sham feeding in the rat. Pharmacol Biochem Behav 8:405-407.

Marini P, Cowie P, Ayar A, Bewick GS, Barrow J, Pertwee RG, MacKenzie A, Tucci P (2023) M3 Receptor Pathway Stimulates Rapid Transcription of the CB1 Receptor Activation through Calcium Signalling and the CNR1 Gene Promoter. Int J Mol Sci 24.

Mawe G, Lavoie B, Nelson M, Pozo M (2018) Neuromuscular Function in the Biliary Tract. In: Physiology of the Gastrointestinal Tract (Said H, ed), pp 453-468: Elsevier/Academic Press.

McDougle M, Quinn D, Diepenbroek C, Singh A, de la Serre C, de Lartigue G (2021) Intact vagal gut-brain signalling prevents hyperphagia and excessive weight gain in response to high-fat high-sugar diet. Acta Physiol (Oxf) 231:e13530.

Muise ED, Gandotra N, Tackett JJ, Bamdad MC, Cowles RA (2017) Distribution of muscarinic acetylcholine receptor subtypes in the murine small intestine. Life sciences 169:6-10.

Perrin-Terrin A, Jeton F, Pichon A, Frugiere A, Richalet J, Bodineau L, Voituron N (2016) The c-FOS Protein Immunohistological Detection: A Useful Tool As a Marker of Central Pathways Involved in Specific Physiological Responses In Vivo and Ex Vivo. Jove-Journal of Visualized Experiments.

Peter JC, Tugler J, Eftekhari P, Maurice D, Hoebeke J, Roegel JC (2005) Effects on heart rate of an anti-M2 acetylcholine receptor immune response in mice. FASEB J 19:943-949.

Piomelli D, Astarita G, Rapaka R (2007) A neuroscientist's guide to lipidomics. Nature reviews 8:743-754.

Pradhan SN, Roth T (1968) Comparative behavioral effects of several anticholinergic agents in rats. Psychopharmacologia 12:358-366.

Rinaldo L, Hansel C (2013) Muscarinic acetylcholine receptor activation blocks long-term potentiation at cerebellar parallel fiber-Purkinje cell synapses via cannabinoid signaling. Proceedings of the National Academy of Sciences of the United States of America 110:11181-11186.

Rogers R, Hermann G, Travagli R, Johnson L (2006) Brainstem Control of Gastric Function. Physiology of the Gastrointestinal Tract, Vols 1 and 2, 4th Edition:851-875.

Ruiz de Azua I, Gautam D, Guettier JM, Wess J (2011) Novel insights into the function of β-cell M3 muscarinic acetylcholine receptors: therapeutic implications. Trends Endocrinol Metab 22:74-80.
Schindelin J, Arganda-Carreras I, Frise E, Kaynig V, Longair M, Pietzsch T, Preibisch S, Rueden C, Saalfeld S, Schmid B, Tinevez J, White D, Hartenstein V, Eliceiri K, Tomancak P, Cardona A (2012) Fiji: an open-source platform for biological-image analysis. Nature Methods 9:676-682.
Schubert M, Peura D (2008) Control of gastric acid secretion in health and disease. Gastroenterology 134:1842-1860.
Sclafani A (2018) From appetite setpoint to appetition: 50years of ingestive behavior research. Physiol Behav 192:210-217.
Sohn JW, Harris LE, Berglund ED, Liu T, Vong L, Lowell BB, Balthasar N, Williams KW, Elmquist JK (2013) Melanocortin 4 receptors reciprocally regulate sympathetic and parasympathetic preganglionic neurons. Cell 152:612-619.
Stella N, Schweitzer P, Piomelli D (1997) A second endogenous cannabinoid that modulates long-term potentiation. Nature 388:773-778.
Straiker A, Mackie K (2007) Metabotropic suppression of excitation in murine autaptic hippocampal neurons. The Journal of physiology 578:773-785.
Sykaras AG, Demenis C, Case RM, McLaughlin JT, Smith CP (2012) Duodenal enteroendocrine I-cells contain mRNA transcripts encoding key endocannabinoid and fatty acid receptors. PLoS ONE 7:e42373.
Tao J, Campbell J, Tsai L, Wu C, Liberles S, Lowell B (2021) Highly selective brain-to-gut communication via genetically defined vagus neurons. Neuron 109:2106-+.
Wiley M, Perez P, Argueta D, Avalos B, Wood C, DiPatrizio N (2021) UPLC-MS/MS Method for Analysis of Endocannabinoid and Related Lipid Metabolism in Mouse Mucosal Tissue. Frontiers in Physiology 12.
Wiley MB, DiPatrizio NV (2022) Diet-Induced Gut Barrier Dysfunction Is Exacerbated in Mice Lacking Cannabinoid 1 Receptors in the Intestinal Epithelium. Int J Mol Sci 23.
Williams KW, Elmquist JK (2012) From neuroanatomy to behavior: central integration of peripheral signals regulating feeding behavior. Nature neuroscience 15:1350-1355.
Zhang C, Barkholt P, Nielsen J, Thorbek D, Rigbolt K, Vrang N, Woldbye D, Jelsing J (2020) The dorsomedial hypothalamus and nucleus of the solitary tract as key regulators in a rat model of chronic obesity. Brain Research 1727.
Zhao Y, Tzounopoulos T (2011) Physiological activation of cholinergic inputs controls associative synaptic plasticity via modulation of endocannabinoid signaling. J Neurosci 31:3158-3168.

Figure Legends

Figure 1. Increased cFos immunoreactivity in the DMV of DIO mice. cFos immunoreactivity was quantified in the DMV of mice fed, ***A***, standard diet (SD) and mice fed , ***B,*** western diet (WD) 45-75 minutes following the onset of the dark period. ***C***, The number of $cFos^+$ cells was significantly increased

in WD mice when compared to SD mice ($t_{(10)}$ = 5.575; p = 0.0002; unpaired Student's t test). ***D,*** cFos immunoreactivity (panel 1), ChAT immunoreactivity (panel 2), and merged (panel 3) images of the DMV in SD mice (top row) and WD mice (bottom row). ***E,*** The number of $cFos^+$ cells was significantly increased in the second cohort of WD mice compared to SD controls ($t_{(10)}$ = 2.462; p = 0.0335; unpaired Student's t test). ***F***, The number of cells co-labeled with both cFos and ChAT was significantly increased in the DMV of WD-fed mice ($t_{(10)}$ = 2.342; p = 0.0412; unpaired Student's t test). ***G***, 73.33% of $cFos^+$ cells in WD-fed animals were also immunoreactive for ChAT, while 57.93% of $cFos^+$ cells in SD-fed animals were immunoreactive for ChAT. There was no significant difference in the ratio of $ChAT^+/cFos^+$ cells between WD- and SD-fed groups. All data are presented as mean ± SEM, n = 6 mice per diet, ***p < 0.001. AP = Area Postrema, CC = Central Canal, 4V = Fourth Ventricle.

Figure 2. Mice fed western diet (WD) become obese and hyperphagic. ***A***, Body weight was recorded bi-weekly between 0900h and 1000h (time x diet interaction: $F_{(16,480)}$ = 121.8; p < 0.0001; diet main effect $F_{(1,30)}$ = 79.56; p < 0.0001; 2-way ANOVA followed by Holm Sidak's multiple comparisons test). ***B***, Change in body mass (time x diet interaction: $F_{(16,480)}$ = 121.8; p < 0.0001; diet main effect $F_{(1,30)}$ = 195.4; p < 0.0001; 2-way ANOVA followed by Holm Sidak's multiple comparisons test). ***C***, Total caloric intake during a 24 h test period ($t_{(30)}$ = 3.666; p = 0.0009; unpaired Student's t test). ***D***, At the end of the 60-day diet exposure period to western diet (WD), epididymal fat pads were weighed ($t_{(30)}$ = 9.686; p > 0.0001; unpaired Student's t test). All data are presented as mean ± SEM, n = 16 per diet; *p < 0.05, **p < 0.01, ***p < 0.001, ****p < 0.0001.

Figure 3. mAChR antagonists block MAG formation in the jejunum epithelium of DIO mice. Mice fed standard diet (SD) or western diet (WD) were treated with a single IP injection of vehicle, DAU5884 (2

mg/kg) or PIR (2 mg/kg) 30 minutes prior to tissue harvest (cohort 1). A second group (cohort 2) of WD mice was treated with vehicle or ATR (2 mg/kg), and otherwise processed identically to cohort 1. ***A***, 2-AG and other MAGs in upper small-intestinal epithelium tissue were isolated via lipid extraction and quantitated using UPLC-MS/MS. 2-AG was significantly elevated in vehicle-treated WD mice when compared to vehicle-treated SD mice. Treatment with DAU or ATR in WD mice restored levels of 2-AG to levels in SD control mice (cohort 1: $F_{(3,28)} = 3.721$, $P = 0.0227$; SD vehicle vs. WD vehicle $p = 0.0448$; WD vehicle vs WD DAU $p = 0.0402$; 1-way ANOVA followed by Holm Sidak's multiple comparisons test; cohort 2: $t_{(18)} = 2.510$; $p = 0.0218$; unpaired Student's t test). ***B***, 2-DG was significantly elevated in vehicle-treated WD mice compared to vehicle-treated SD mice. Treatment with DAU or ATR in WD mice restored levels of 2-AG to that of SD mice (cohort 1: $F_{(3,28)} = 4.691$, $P = 0.0089$; SD vehicle vs. WD vehicle $p = 0.0200$; WD vehicle vs WD DAU $p = 0.0159$; 1-way ANOVA followed by Holm Sidak's multiple comparisons test; cohort 2: $t_{(18)} = 2.115$; $p = 0.0486$; unpaired Student's t test). ***C,*** 2-OG was significantly elevated in vehicle-treated WD mice when compared to vehicle-treated SD mice. Treatment with DAU or PIR restored levels of 2-AG in WD mice to those in SD mice (cohort 1: $F_{(3,25)} = 6.657$, $P = 0.0019$; SD vehicle vs. WD vehicle $p = 0.0014$; WD vehicle vs WD DAU $p = 0.0439$; WD vehicle vs WD PIR $p = 0.0315$; 1-way ANOVA followed by Holm Sidak's multiple comparisons test; cohort 2: $t_{(17)} = 1.565$; $p = 0.1361$; unpaired Student's t test). ***D,*** 2-LG levels were not significantly different between any treatment or diet groups (cohort 1: $F_{(3,25)} = 3.346$, $P = 0.0351$; SD vehicle vs. WD vehicle $p = 0.0014$; WD vehicle vs WD DAU $p = 0.0439$; WD vehicle vs WD PIR $p = 0.0315$; 1-way ANOVA followed by Holm Sidak's multiple comparisons test; cohort 2: $t_{(18)} = 1.720$; $p = 0.1026$; unpaired Student's t test). All data are presented as mean ± SEM, n = 8-10 per group; $*p < 0.05$, $**p < 0.01$.

Figure 4. Pirenzepine dose response analysis. Doses of PIR within one log step of the original 2 mg per kg dose were tested for their ability to inhibit MAG formation in the upper intestinal epithelium and

attenuate food intake in WD-fed animals. ***A,*** 2.0 mg per kg of PIR significantly reduced 2-AG levels compared to the vehicle and 0.65 mg per kg dose ($F_{(3,12)}$ = 0.310, P = 0.0150; 0.0 vs. 2.0 p = 0.0265; 0.65 vs 2.0 p = 0.0265). ***B,*** 2.0 mg per kg of PIR significantly reduced 2-DG levels compared to the vehicle and 0.65 mg per kg dose ($F_{(3,12)}$ = 0.8774, P = 0.0124; 0.0 vs. 2.0 p = 0.0227; 0.65 vs 2.0 p = 0.0212). ***C,*** PIR did not affect 2-OG levels at any dose ($F_{(3,12)}$ = 0.635, P = 0.1046). ***D,*** PIR did not affect 2-LG levels at any dose ($F_{(3,12)}$ = 0.126, P = 0.0847). ***E,*** There was a main effect of time and PIR dose on food intake, but no significant differences were detected in the multiple comparisons test (time main effect $F_{(3, 224)}$ = 43.44; p < 0.0001, dose main effect $F_{(3, 224)}$ = 3.516; p = 0.02). ***F***, There was a main effect of time, but not dose, on water intake, but no significant differences were detected in the multiple comparisons test (time main effect $F_{(3, 224)}$ = 42.31; p < 0.001). ***G,*** There was a main effect of time, but not dose, on ambulation, but no significant differences were detected in the multiple comparisons test (time main effect $F_{(3, 224)}$ = 32.23; p < 0.0001). ***A-D*** are 1-way ANOVAs followed by Holm-Sidak's multiple comparisons test when appropriate, n = 4 per dose, ***E-G*** are 2-way ANOVAs followed by Holm-Sidak's multiple comparisons test when appropriate, n = 15. All data are presented as mean ± SEM; *p < 0.05.

Figure 5. SAG formation and DGL Activity in upper intestinal epithelium are inhibited by mAChR antagonism in DIO mice. Levels of SAG in the upper small-intestinal epithelium tissue were isolated and quantitated using UPLC-MS/MS. The same tissue was analyzed for DGL and MGL activity using an enzymatic assay; enzyme reaction products were isolated and quantitated via UPLC-MS/MS. Enzyme activity was calculated using the nmols of reaction product generated per mg of tissue per minute of the reaction. ***A,*** SAG was significantly elevated in vehicle-treated mice fed western diet (WD) compared to vehicle-treated mice fed standard diet (SD). Treatment with DAU, PIR, or ATR in WD mice restored levels of SAG to that of lean controls (cohort 1: $F_{(3,27)}$ = 14.76, P < 0.0001; SD Veh vs. WD Veh p = 0.0004; WD Veh vs WD DAU p < 0.0001; WD Veh vs WD PIR p < 0.0001; 1-way ANOVA followed by Holm Sidak's

multiple comparisons test; cohort 2: $t_{(18)} = 5.010$; $p = 0<0.0001$; unpaired Student's *t* test). ***B,*** DGL activity was significantly elevated in vehicle-treated WD mice compared to vehicle-treated SD mice. Treatment with DAU, PIR, or ATR in WD mice restored DGL activity to that of lean controls (cohort 1: $F_{(3,26)} = 10.57$, $P = 0.0001$; SD Veh vs. WD Veh $p = 0.0030$; WD Veh vs WD DAU $p = 0.0013$; WD Veh vs WD PIR $p = 0.0001$; 1-way ANOVA followed by Holm Sidak's multiple comparisons test; cohort 2: $t_{(17)} = 2.546$; $p = 0.0209$; unpaired Student's *t* test). ***C,*** MGL activity was not different between any diet or treatment group (cohort 1: $F_{(3,27)} = 2.537$, $P = 0.0777$; 1-way ANOVA; cohort 2: $t_{(18)} = 2.081$; $p = 0.0520$; unpaired Student's *t* test). All data are presented as mean ± SEM, n = 8-10 per group; $*p < 0.05$, $**p < 0.01$, $***p < 0.001$, $****p < 0.0001$. ***D,*** Schematic illustrating that activation of G_q-coupled mAChRs initiates the PLC-dependent generation of SAG, which is subsequently converted to 2-AG by DGL. 2-AG is further hydrolyzed by MGL into glycerol and arachidonic acid. Illustration created with BioRender.com

Figure 6. Anticholinergics do not affect 2-AG metabolic enzyme activity *ex vivo.* Activity of DGL in the upper small-intestinal epithelium from mice fed western diet (WD) was assayed in the presence increasing concentrations of a DGL-specific inhibitor and various mAChR antagonists. ***A,*** DGL activity was inhibited in a concentration-dependent manner when incubated with THL at concentrations ranging from 3-1,000 nM ($IC_{50} = 58.52$ nM, $R^2 = 0.9499$). ***B,*** DGL activity was not directly inhibited by ATR at concentrations ranging from 10-10,000 nM ($R^2 = -0.0212$). ***C,*** DGL activity was not directly inhibited by DAU at concentrations ranging from 10-10,000 nM ($R^2 = -0.0286$). ***D,*** DGL activity was not directly inhibited by PIR at concentrations ranging from 10-10,000 nM ($R^2 = -0.0113$). All data are presented as mean ± SEM, n = 3 animals per drug. All graphs are least squares fit of log[inhibitor] vs. normalized response.

Figure 7. Anticholinergics inhibit food intake in DIO mice. ***A,*** AM6545 (10 mg/kg), ATR (2 mg/kg), or a combination of AM6545 + ATR reduced caloric intake for up to 24 hours in western diet-fed (WD) mice (time x drug interaction: $F_{(9,158)} = 4.639$; $p < 0.0001$; drug main effect $F_{(3,54)} = 4.560$; $p = 0.0064$; 12 hour vehicle vs. 12 hour ATR $p = 0.0175$, 12 hour vehicle vs. 12 hour AM6545 $p = 0.0143$, 12 hour vehicle vs. 12 hour combination $p = 0.0020$, 24 hour vehicle vs. 24 hour ATR $p = 0.0301$, 24 hour vehicle vs. 24 hour AM6545 $p = 0.0145$, 24 hour vehicle vs. 24 hour combination $p = 0.0049$; 2-way ANOVA followed by Holm Sidak's multiple comparisons test). ***B,*** AM6545, ATR, or both drugs in combination did not affect caloric intake in standard diet-fed (SD) mice (time x drug interaction: $F_{(9,164)} = 0.9117$; $p = 0.5165$; time main effect $F_{(2.103,115.0)} = 142.4$; $p < 0.0001$; drug main effect $F_{(3,56)} = 1.69$; $p = 0.1799$; 2-way ANOVA). ***C,*** DAU5884 (2 mg/kg) reduced caloric intake for up to 12 hours in WD mice (time x drug interaction: $F_{(3,84)} = 1.239$; $p = 0.3009$; drug main effect $F_{(1,28)} = 6.750$; $p = 0.0148$; 1 hour vehicle vs. 1 hour DAU $p = 0.0358$, 6 hour vehicle vs. 6 hour DAU $p = 0.0168$, 12 hour vehicle vs. 12 hour DAU $p = 0.0358$; 2-way ANOVA followed by Holm Sidak's multiple comparisons test). ***D,*** DAU5884 did not affect caloric intake in SD mice for 24 hours (time x drug interaction: $F_{(3,70)} = 0.5839$; $p = 0.6276$; drug main effect $F_{(1,24)} = 0.2090$; $p = 0.6517$; 2-way ANOVA). ***E,*** PIR (2 mg/kg) did not affect caloric intake in WD mice (time x drug interaction: $F_{(3,80)} = 1.526$; $p = 0.2140$; drug main effect $F_{(1,28)} = 0.1463$; $p = 0.7050$; 2-way ANOVA)***. F,*** PIR did not affect caloric intake in standard diet-fed mice (time x drug interaction: $F_{(3,79)} = 1.781$; $p = 0.1576$; drug main effect $F_{(1,28)} = 0.07073$; $p = 0.7922$; 2-way ANOVA). All data are presented as mean ± SEM, n = 15 – 16; $*p < 0.05$, $**p < 0.01$.

Figure 8. Effects of drug treatments on ambulation and water intake. Total distance travelled and cumulative water intake was measured by automated feeding chambers for a 24-hour period starting at the onset of the dark cycle (1800h) following a single IP injection of AM6545 (10 mg/kg), ATR (2 mg/kg),

DAU (2 mg/kg), and PIR (2 mg/kg). ***A***, ATR and AM6545 alone or in combination reduced distance travelled for up to 12 h in mice fed western diet (WD). ***C,*** AM6545 resulted in decreased cumulative distance travelled at the 12 h timepoint in mice fed standard diet (SD). AM6545 and ATR combined reduced ambulation across the 24 h test. ***B & D,*** AM6545 and ATR alone combined had no significant effects on water intake across the 24 h test in mice fed SD or WD. ***E & F,*** A single IP injection of DAU yielded no significant effects on distance travelled in mice fed SD or WD. ***G,*** DAU did not significantly affect water intake for the 24 h test in mice fed SD. ***H,*** In mice fed WD and treated with DAU, water intake was affected by drug alone, as well as a time x drug interaction, although there were no significant differences at individual time points as revealed by the Holm-Sidak multiple comparisons test. ***I & J,*** A single IP injection of PIR yielded no significant effects on distance travelled in mice fed SD or WD for the 24 h test. ***K & L,*** Treatment with PIR also had no effect on water intake in mice fed with SD or WD for the 24 h test. 2-Way ANOVA followed by Holm-Sidak's multiple comparisons test when appropriate, see **Table 1** for detailed statistics. All data are presented as mean ± SEM, n = 15 – 16; *$p < 0.05$, **$p < 0.01$, ***$p < 0.001$, ****$p < 0.0001$.

Figure 9. **Inhibiting peripheral CB_1Rs or mAChRs failed to affect food intake in mice conditionally lacking CB_1Rs in the intestinal epithelium.** ***A,*** AM6545 (10 mg/kg) or ATR (2 mg/kg) reduced caloric intake for up to 24 hours in control intCB_1+/+ mice (time x drug interaction: $F_{(6,79)} = 5.099$; $p = 0.0002$; drug main effect $F_{(2,30)} = 6.024$; $p = 0.0063$; 12 hour vehicle vs. 12 hour AM6545 $p = 0.0498$, 24 hour vehicle vs. 24 hour AM6545 $p = 0.0012$, 24 hour vehicle vs. 24 hour ATR $p = 0.0043$, 2-way ANOVA followed by Holm Sidak's multiple comparisons test). ***B,*** AM6545 or ATR did not affect caloric intake in intCB_1-/- mice (time x drug interaction: $F_{(6,135)} = 0.7700$; $p = 0.5948$; drug main effect $F_{(2,45)} = 0.9273$; $p = 0.4030$; 2-way ANOVA). ***C,*** Body weights were similar between intCB_1-/- when compared to intCB_1+/+ mice control mice fed western diet (WD; time x genotype interaction: $F_{(9,225)} = 5.327$; $p < 0.0001$;

genotype main effect $F_{(1,25)}$ = 0.01602; p = 0.9003; 2-way ANOVA followed by Holm Sidak's multiple comparisons test). ***D,*** Change in body weight was lower in intCB_1-/- when compared to intCB_1+/+ control mice (time x genotype interaction: $F_{(9,225)}$ = 5.327; $p < 0.0001$; genotype main effect $F_{(1,25)}$ = 5.077; p = 0.0333; 2-way ANOVA followed by Holm Sidak's multiple comparisons test). All data are presented as mean ± SEM, n = 16, 11 (intCB_1-/-, intCB_1+/+ respectively), $p < 0.05$, $^{**}p < 0.01$.

Figure 10. Effects of drug treatments on ambulation and water intake in mice with conditional deletion of CB_1Rs in the intestinal epithelium fed western diet (WD). ***A-B,*** Total distance travelled and, ***C-D,*** cumulative water intake was measured by automated feeding chambers for a 24-hour period starting at the onset of the dark cycle (1800h) following a single IP injection of AM6545 (10 mg/kg) or ATR (2 mg/kg) in intCB_1+/+ and intCB_1-/- fed WD. ***A,*** A single dose of AM6545 in IntCB_1+/+ controls affected distance travelled across the entire 24-hour testing period. ATR also reduced distance travelled in the same mice at the 1- and 24-hour timepoints. ***B,*** There was a significant effect of drug and drug x time interaction in IntCB_1-/- mice on distance travelled, but the Holm-Sidak multiple comparisons *post hoc* analysis did not reveal any significant differences at individual time points. ***C,*** Water intake of intCB_1+/+ mice was not significantly affected by either drug treatment for the 24 h test. ***D,*** There was a significant effect of drug, as well as a drug x time interaction on water intake inintCB_1-/- animals. Specifically, AM6545 treatment significantly reduced cumulative water intake at the 1-, 6-, and 24-h timepoints. 2-way ANOVA followed by Holm-Sidak's multiple comparisons test when appropriate, see **Table 2** for detailed statistics. All data are presented as mean ± SEM, n = 11 or 16 (intCB_1+/+ and intCB_1-/-, respectively); $^{*}p < 0.05$, $^{**}p < 0.01$, $^{***}p < 0.001$, $^{****}p < 0.0001$.

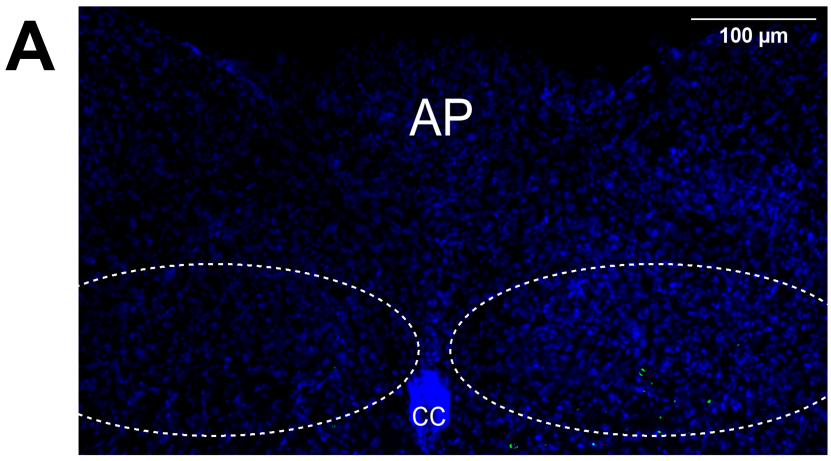
A
100 µm
AP
cc

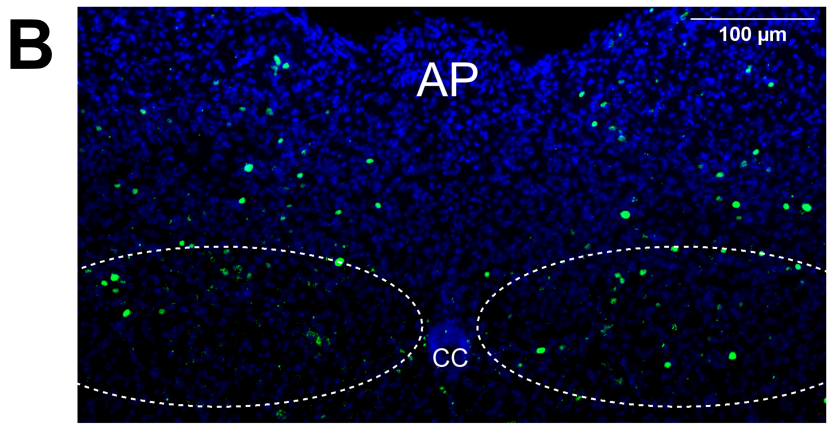
B
100 µm
AP
cc

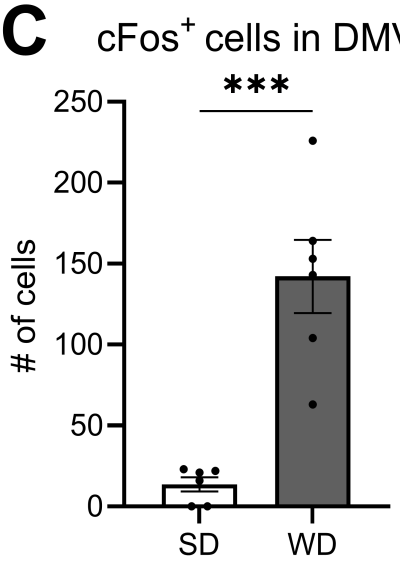
C
cFos+ cells in DMV
***
250
200
150
100
50
0
# of cells
SD
WD

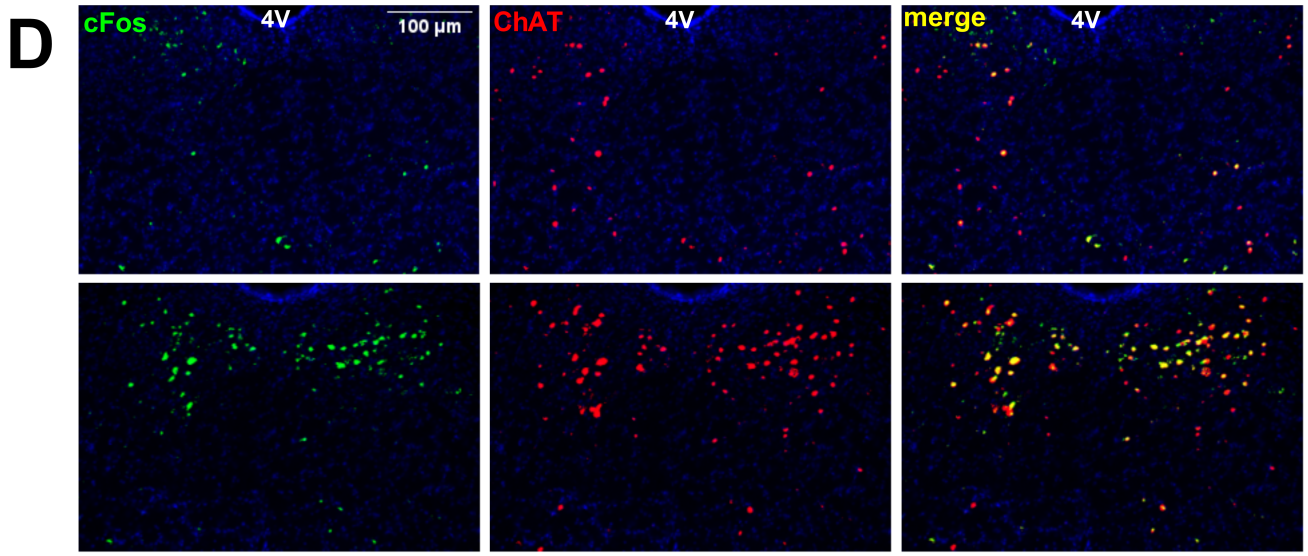
D
cFos
4V
100 µm
ChAT
4V
merge
4V

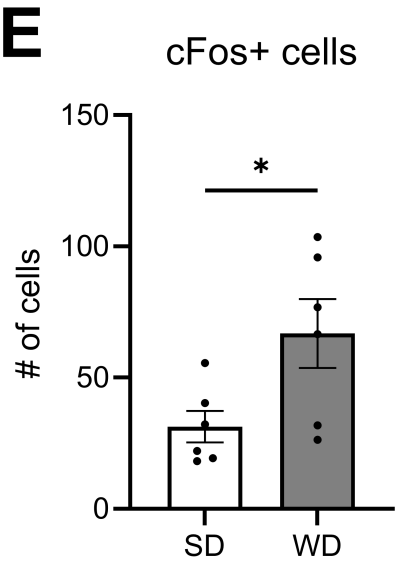
E
cFos+ cells
*
150
100
50
0
# of cells
SD
WD

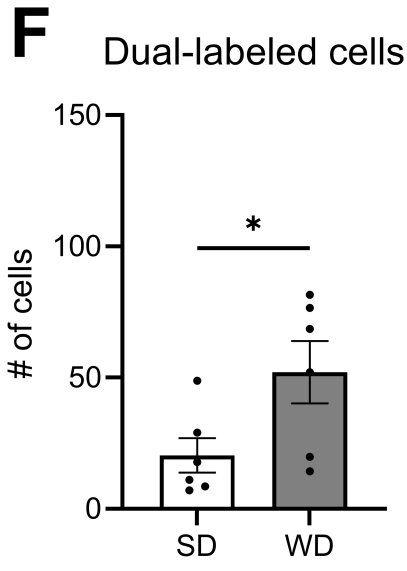
F
Dual-labeled cells
*
150
100
50
0
# of cells
SD
WD

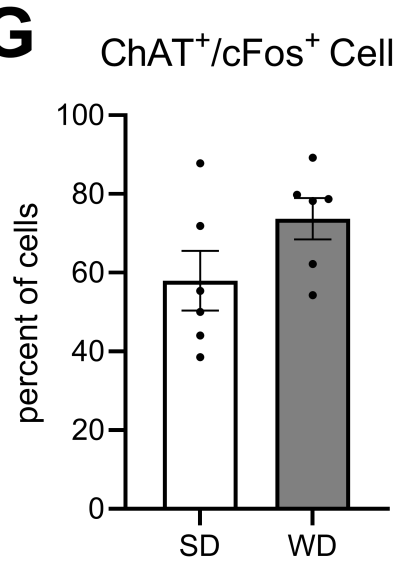
G
ChAT+/cFos+ Cells
100
80
60
40
20
0
percent of cells
SD
WD

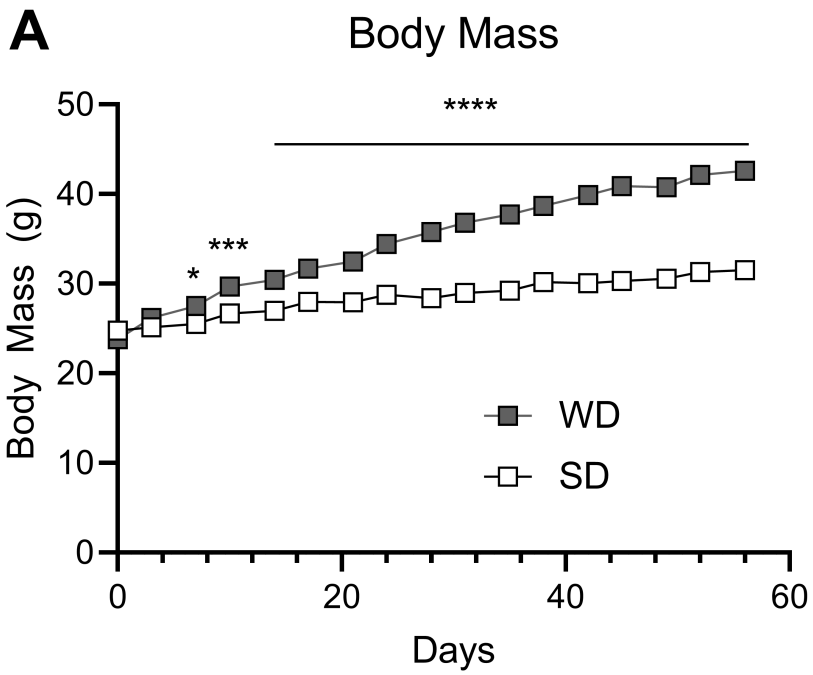
A
Body Mass
Body Mass (g)
Days
WD
SD
****
***
*
0
10
20
30
40
50
0
20
40
60

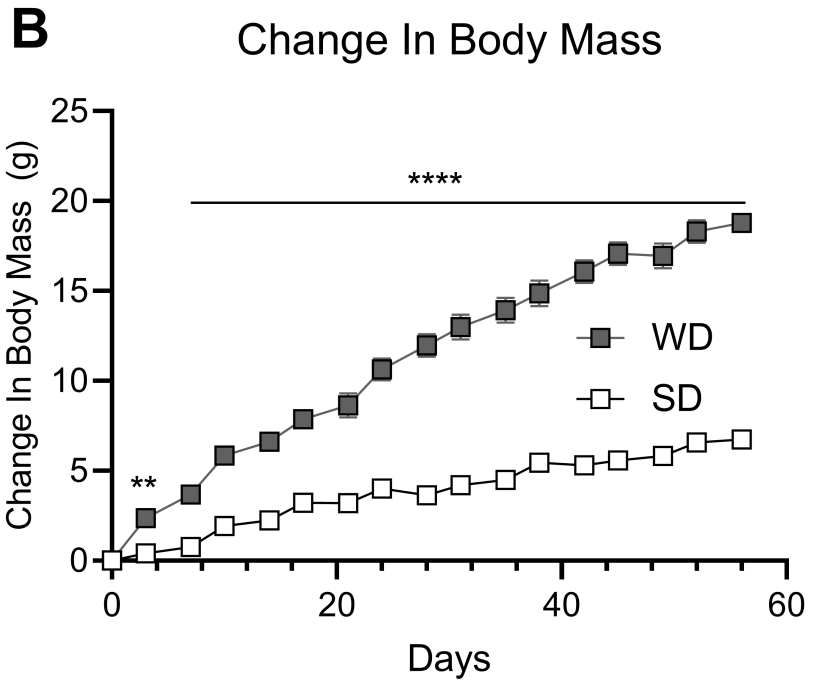
B
Change In Body Mass
Change In Body Mass (g)
Days
WD
SD
****
**
0
5
10
15
20
25
0
20
40
60

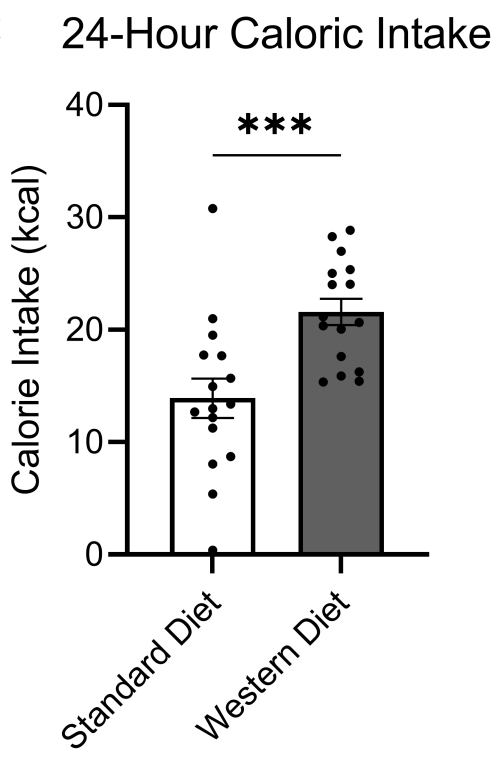
C
24-Hour Caloric Intake
Calorie Intake (kcal)
***
0
10
20
30
40
Standard Diet
Western Diet

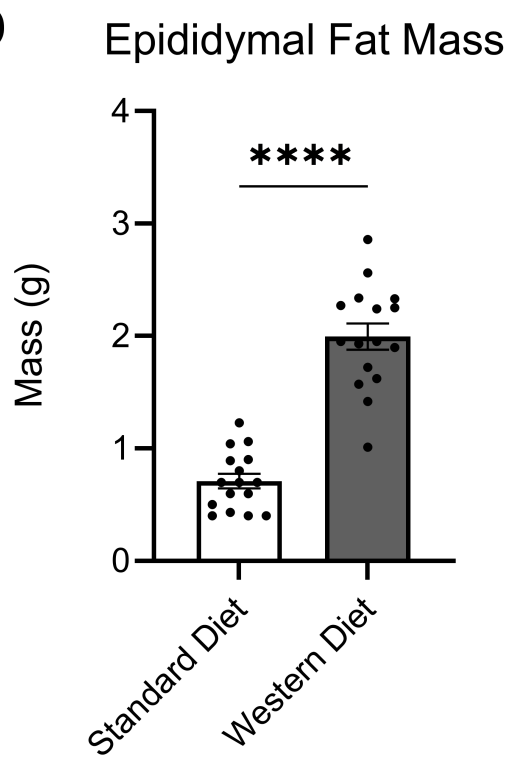
D
Epididymal Fat Mass
Mass (g)
****
0
1
2
3
4
Standard Diet
Western Diet

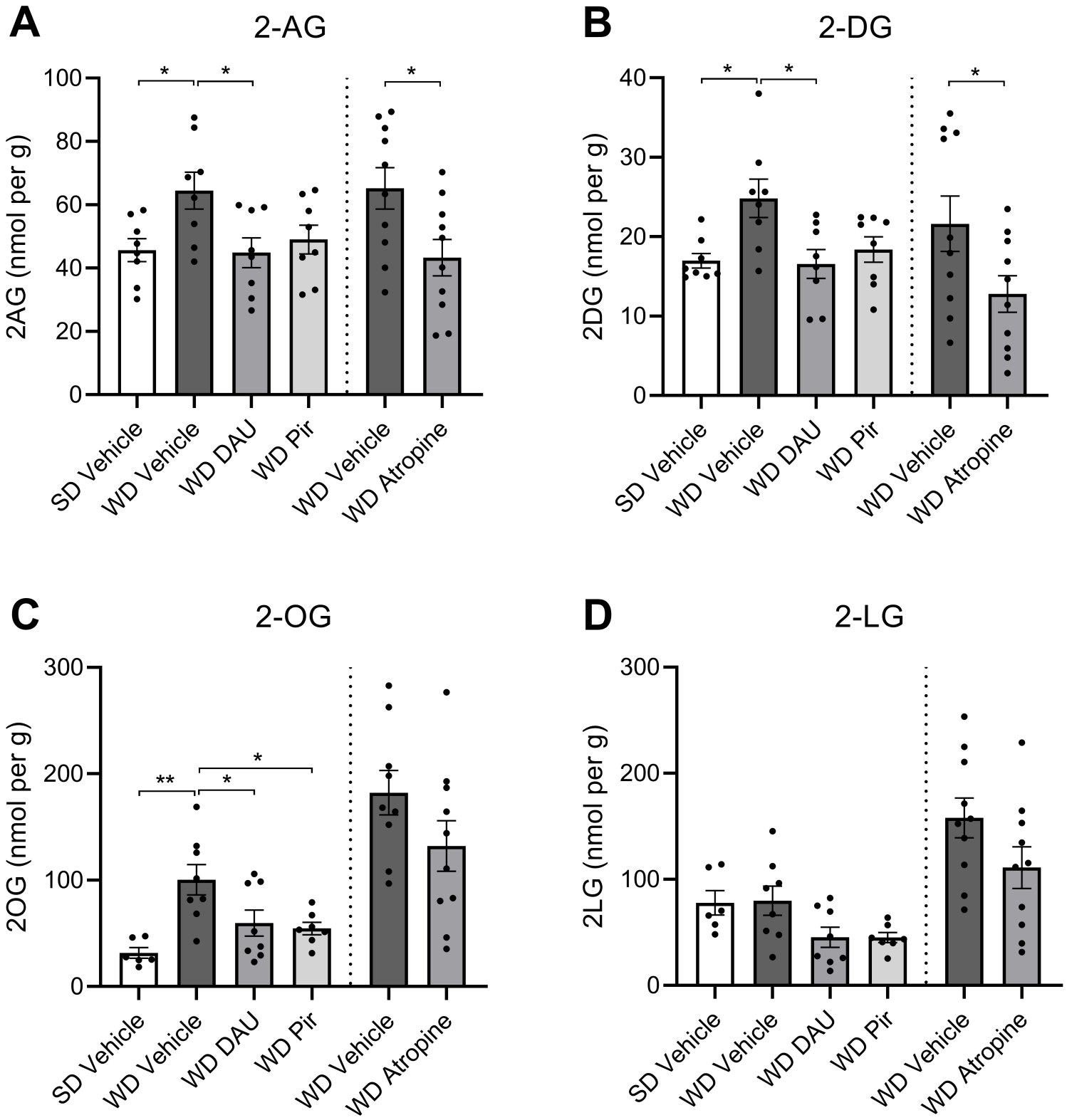
A
2-AG
2AG (nmol per g)
100
80
60
40
20
0
*
*
*
SD Vehicle
WD Vehicle
WD DAU
WD Pir
WD Vehicle
WD Atropine
B
2-DG
2DG (nmol per g)
40
30
20
10
0
*
*
*
SD Vehicle
WD Vehicle
WD DAU
WD Pir
WD Vehicle
WD Atropine
C
2-OG
2OG (nmol per g)
300
200
100
0
**
*
*
SD Vehicle
WD Vehicle
WD DAU
WD Pir
WD Vehicle
WD Atropine
D
2-LG
2LG (nmol per g)
300
200
100
0
SD Vehicle
WD Vehicle
WD DAU
WD Pir
WD Vehicle
WD Atropine

A

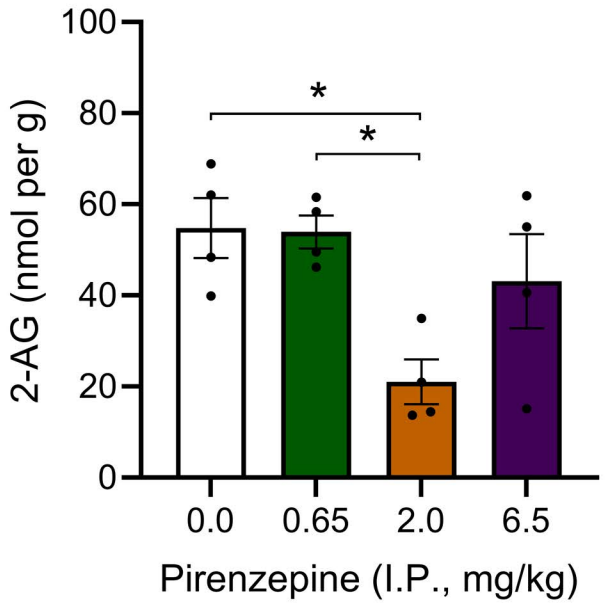
2-AG
2-AG (nmol per g)
100
80
60
40
20
0
*
*
0.0
0.65
2.0
6.5
Pirenzepine (I.P., mg/kg)

B

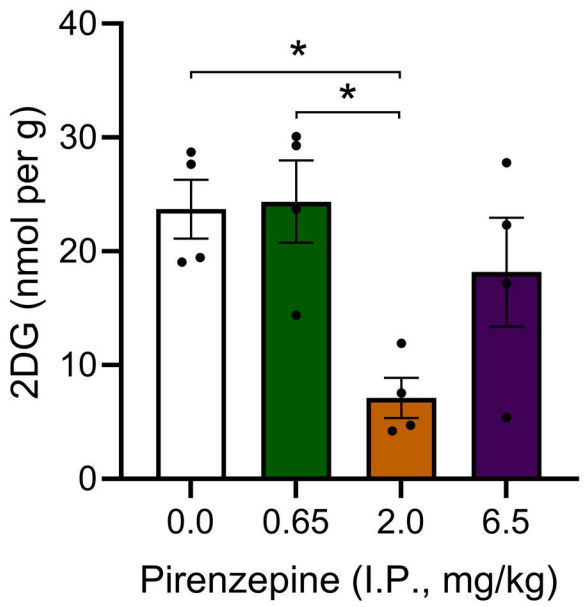
2-DG
2DG (nmol per g)
40
30
20
10
0
*
*
0.0
0.65
2.0
6.5
Pirenzepine (I.P., mg/kg)

C

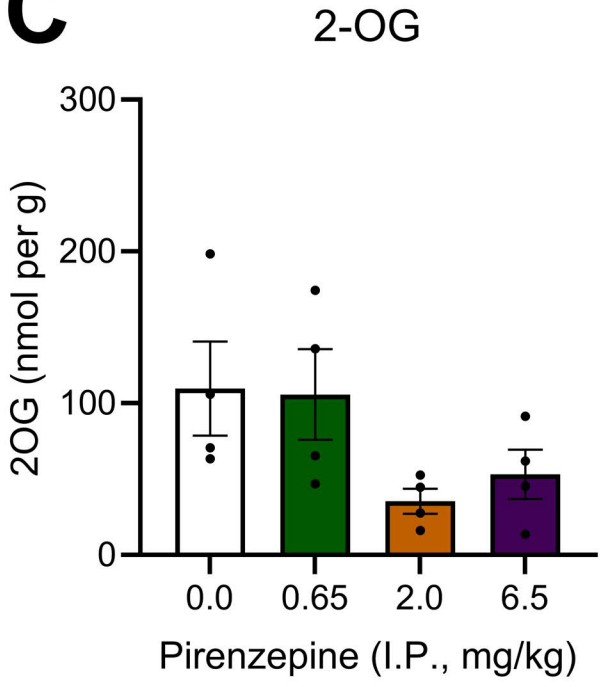
2-OG
2OG (nmol per g)
300
200
100
0
0.0
0.65
2.0
6.5
Pirenzepine (I.P., mg/kg)

D

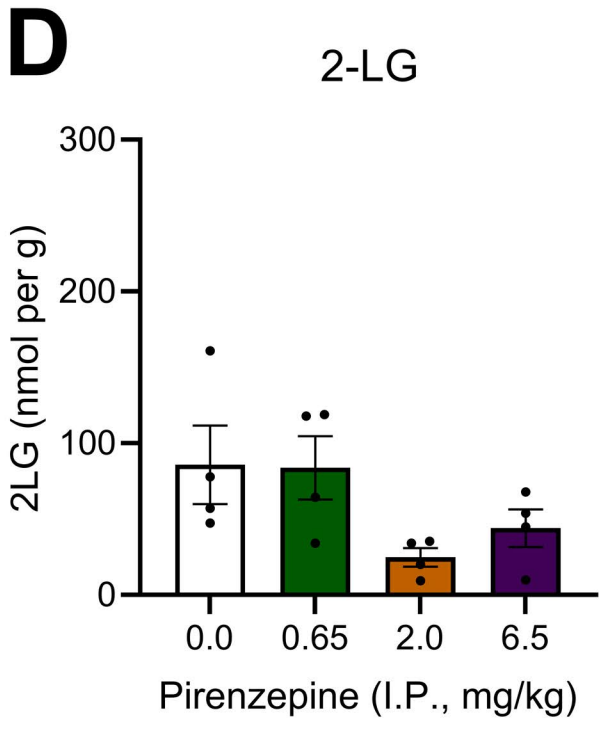
2-LG
2LG (nmol per g)
300
200
100
0
0.0
0.65
2.0
6.5
Pirenzepine (I.P., mg/kg)

E

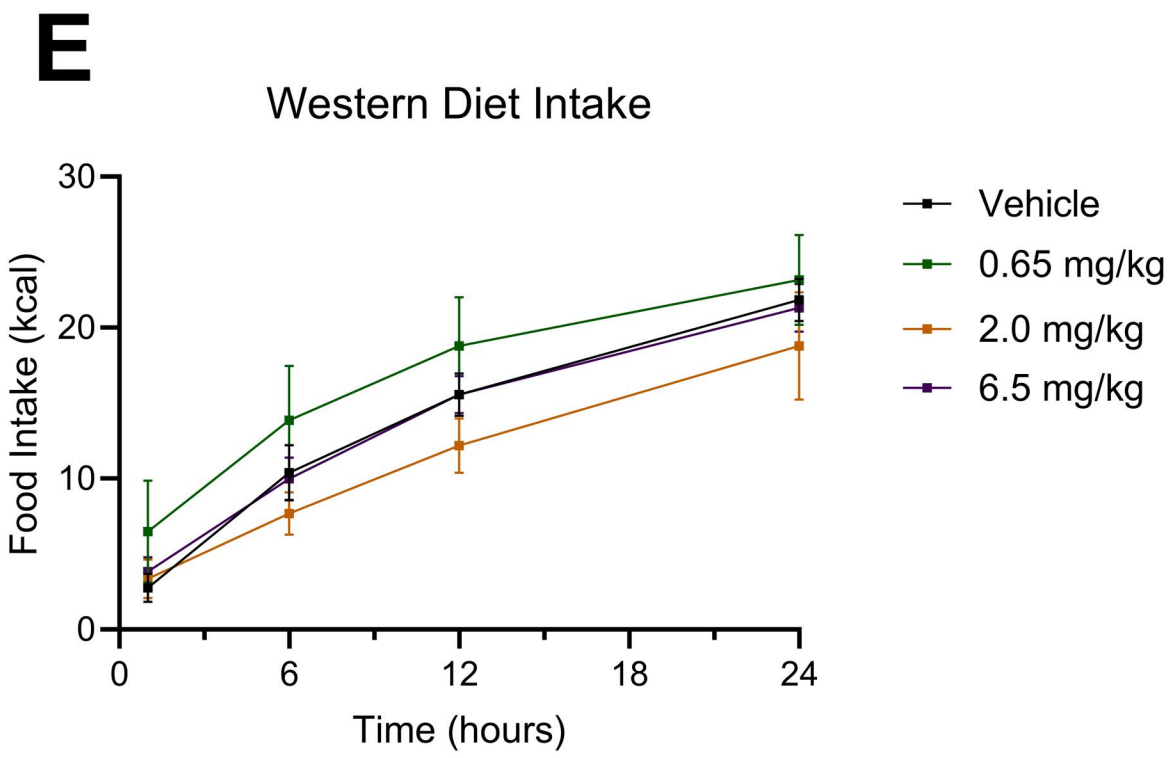
Western Diet Intake
Food Intake (kcal)
30
20
10
0
0
6
12
18
24
Time (hours)
Vehicle
0.65 mg/kg
2.0 mg/kg
6.5 mg/kg

F

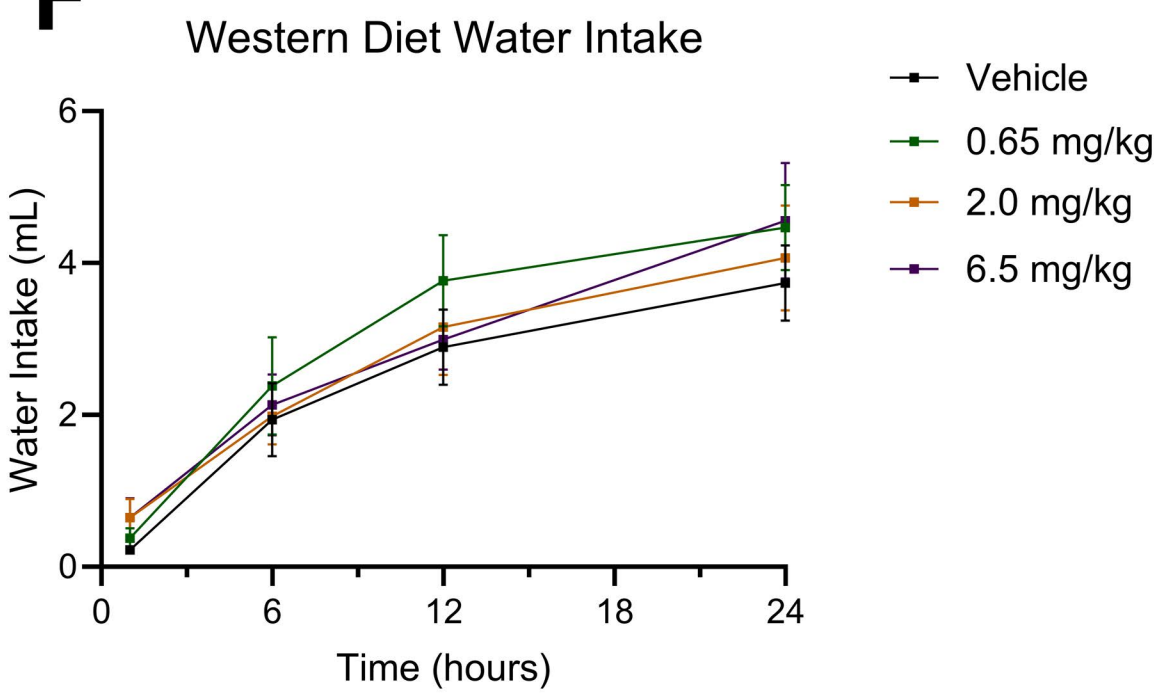
Western Diet Water Intake
Water Intake (mL)
6
4
2
0
0
6
12
18
24
Time (hours)
Vehicle
0.65 mg/kg
2.0 mg/kg
6.5 mg/kg

G

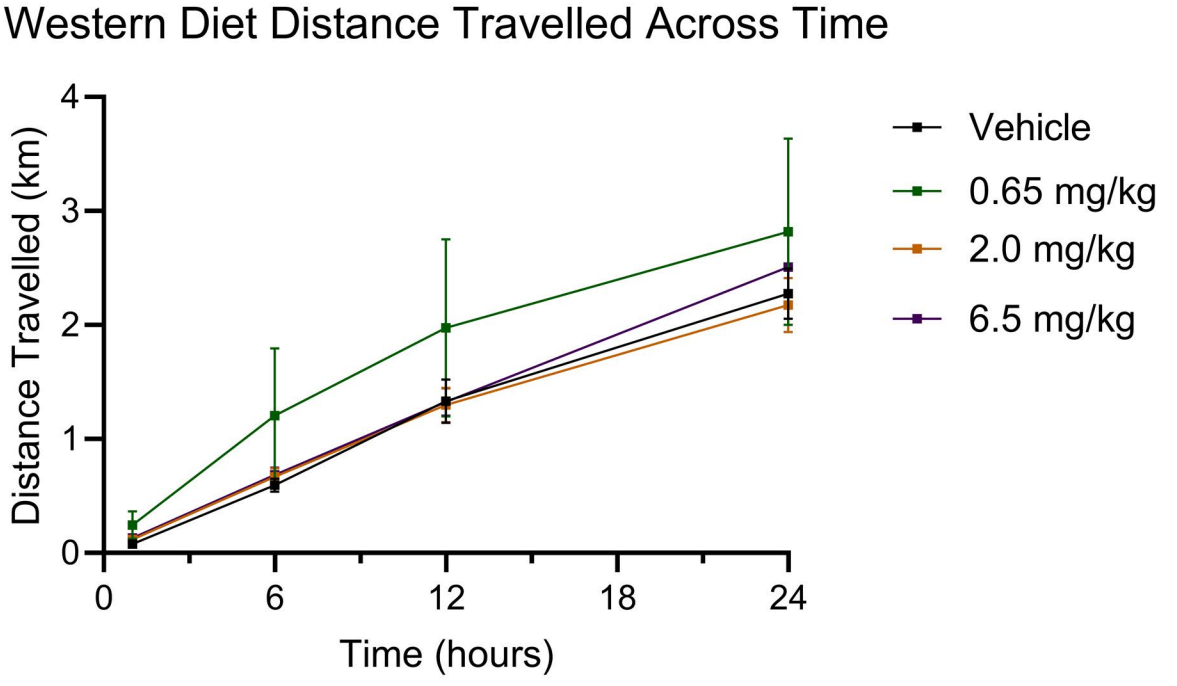
Western Diet Distance Travelled Across Time
Distance Travelled (km)
4
3
2
1
0
0
6
12
18
24
Time (hours)
Vehicle
0.65 mg/kg
2.0 mg/kg
6.5 mg/kg

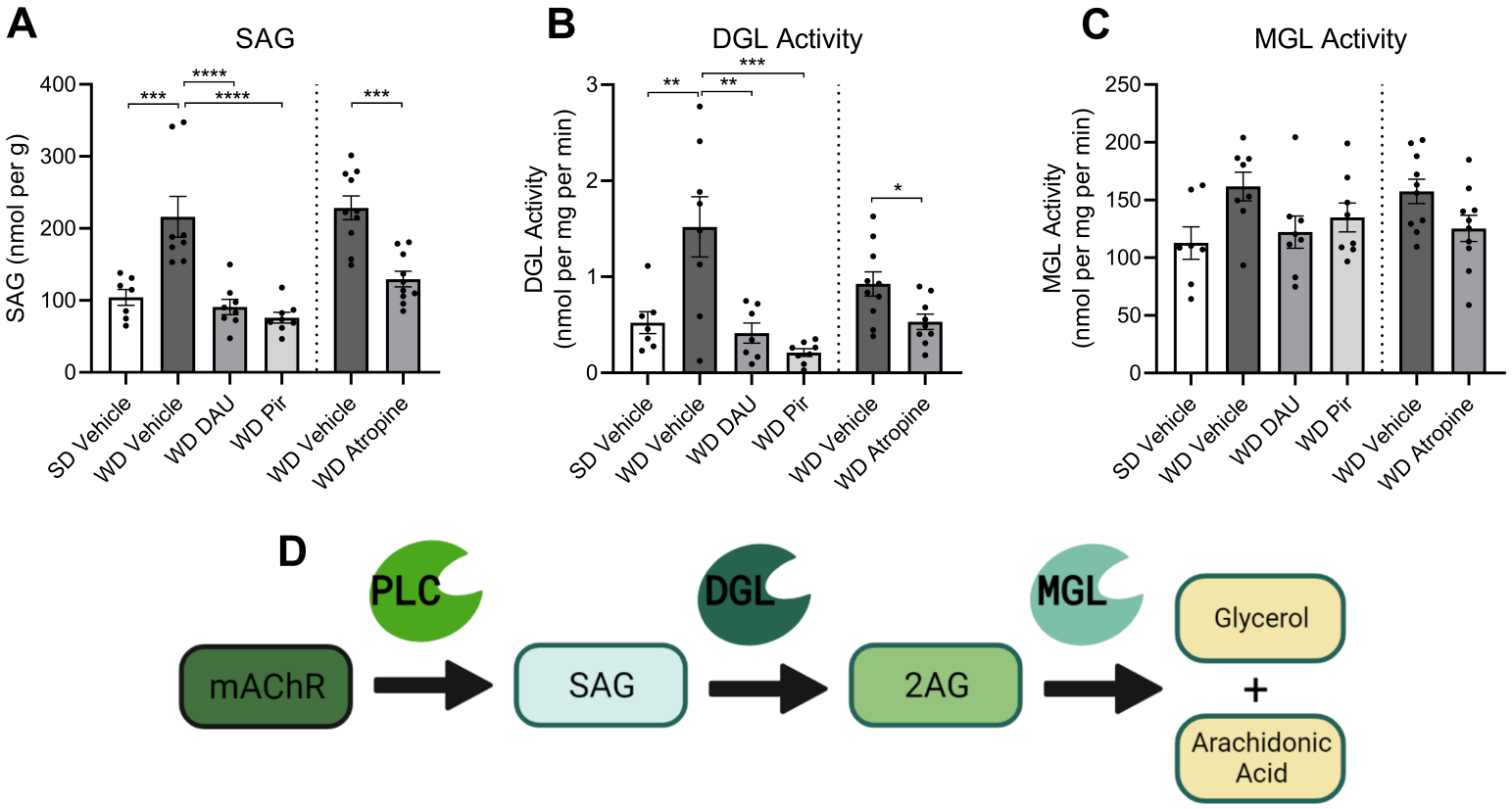
A
SAG
SAG (nmol per g)
400
300
200
100
0
***
****
****
***
SD Vehicle
WD Vehicle
WD DAU
WD Pir
WD Vehicle
WD Atropine
B
DGL Activity
DGL Activity
(nmol per mg per min)
3
2
1
0
**
**
***
*
SD Vehicle
WD Vehicle
WD DAU
WD Pir
WD Vehicle
WD Atropine
C
MGL Activity
MGL Activity
(nmol per mg per min)
250
200
150
100
50
0
SD Vehicle
WD Vehicle
WD DAU
WD Pir
WD Vehicle
WD Atropine
D
PLC
DGL
MGL
mAChR
SAG
2AG
Glycerol
+
Arachidonic
Acid

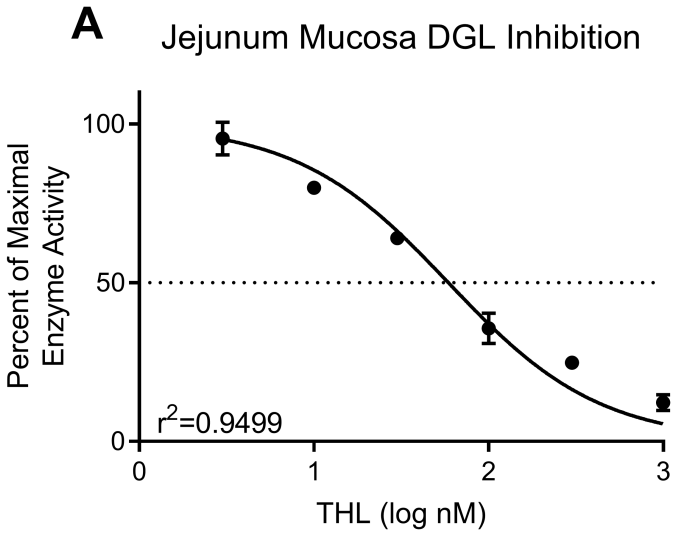
A
Jejunum Mucosa DGL Inhibition
Percent of Maximal Enzyme Activity
100
50
0
r2=0.9499
0
1
2
3
THL (log nM)

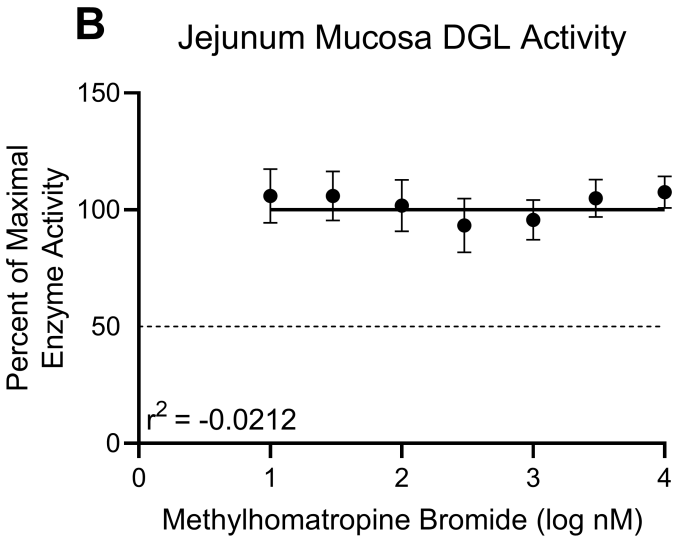
B
Jejunum Mucosa DGL Activity
Percent of Maximal Enzyme Activity
150
100
50
0
r2 = -0.0212
0
1
2
3
4
Methylhomatropine Bromide (log nM)

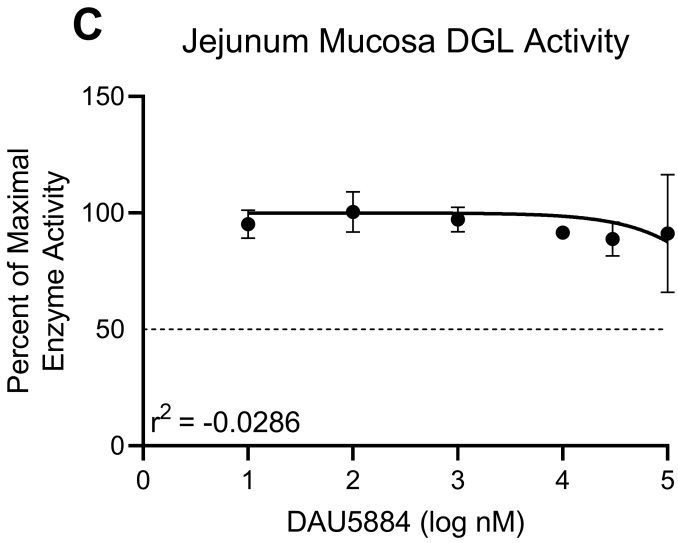
C
Jejunum Mucosa DGL Activity
Percent of Maximal Enzyme Activity
150
100
50
0
r2 = -0.0286
0
1
2
3
4
5
DAU5884 (log nM)

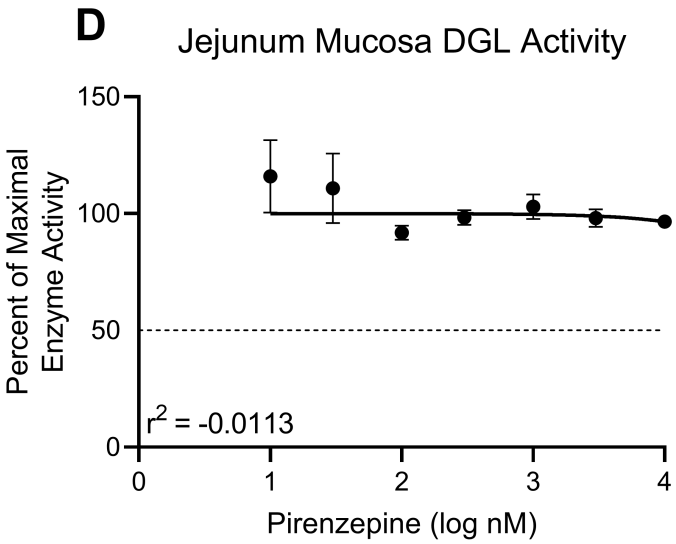
D
Jejunum Mucosa DGL Activity
Percent of Maximal Enzyme Activity
150
100
50
0
r2 = -0.0113
0
1
2
3
4
Pirenzepine (log nM)

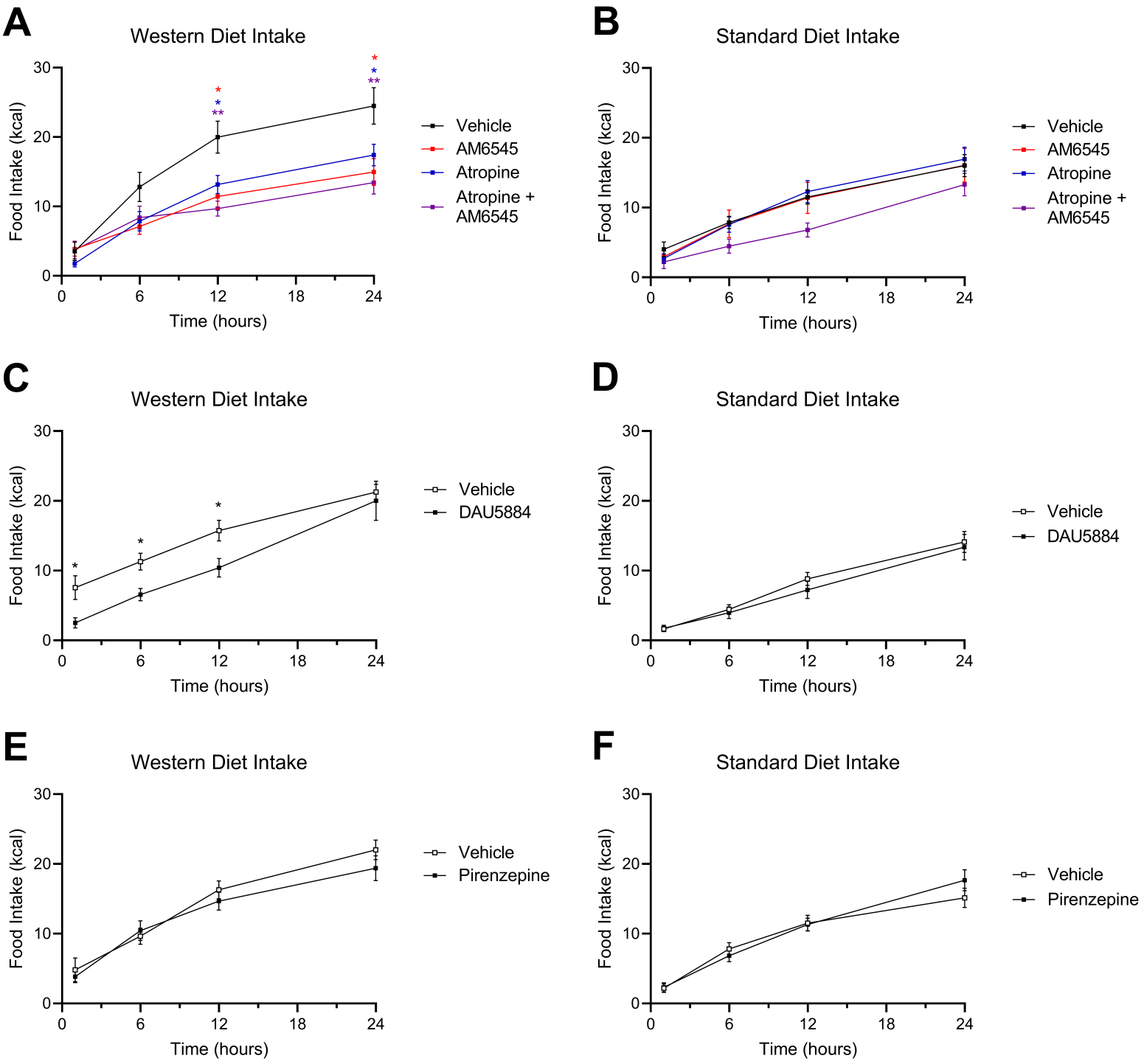
A
Western Diet Intake
Food Intake (kcal)
Time (hours)
Vehicle
AM6545
Atropine
Atropine + AM6545
B
Standard Diet Intake
Food Intake (kcal)
Time (hours)
Vehicle
AM6545
Atropine
Atropine + AM6545
C
Western Diet Intake
Food Intake (kcal)
Time (hours)
Vehicle
DAU5884
D
Standard Diet Intake
Food Intake (kcal)
Time (hours)
Vehicle
DAU5884
E
Western Diet Intake
Food Intake (kcal)
Time (hours)
Vehicle
Pirenzepine
F
Standard Diet Intake
Food Intake (kcal)
Time (hours)
Vehicle
Pirenzepine

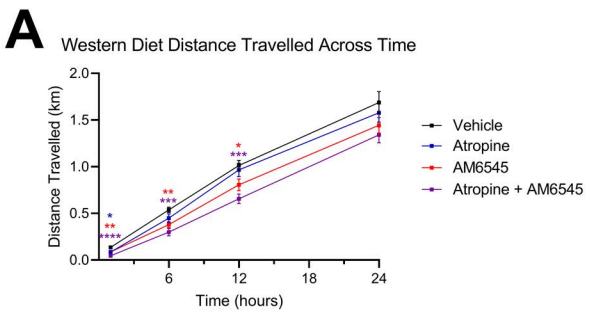
A
Western Diet Distance Travelled Across Time
Distance Travelled (km)
Time (hours)
Vehicle
Atropine
AM6545
Atropine + AM6545

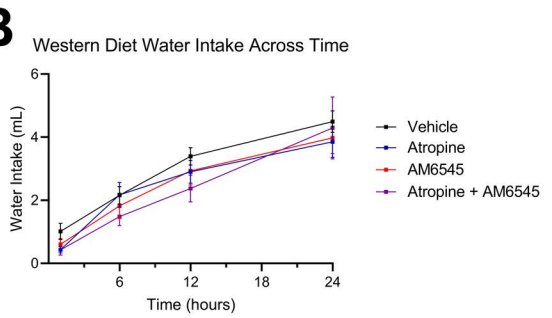
B
Western Diet Water Intake Across Time
Water Intake (mL)
Time (hours)
Vehicle
Atropine
AM6545
Atropine + AM6545

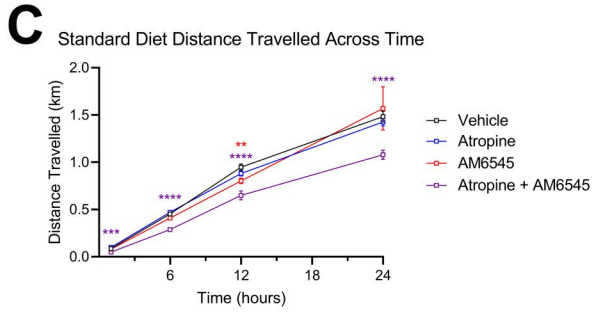
C
Standard Diet Distance Travelled Across Time
Distance Travelled (km)
Time (hours)
Vehicle
Atropine
AM6545
Atropine + AM6545

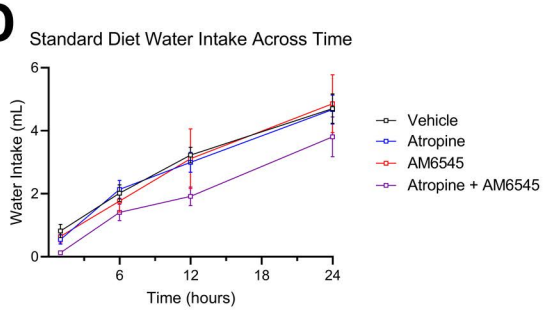
D
Standard Diet Water Intake Across Time
Water Intake (mL)
Time (hours)
Vehicle
Atropine
AM6545
Atropine + AM6545

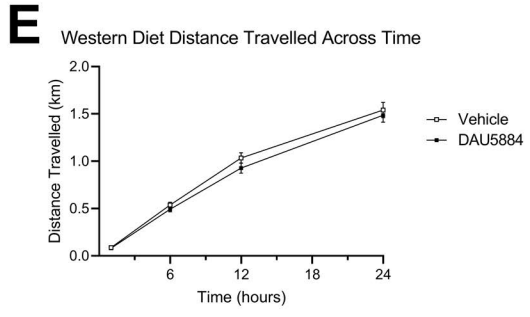
E
Western Diet Distance Travelled Across Time
Distance Travelled (km)
Time (hours)
Vehicle
DAU5884

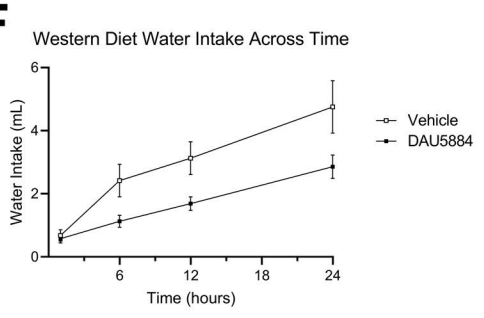
F
Western Diet Water Intake Across Time
Water Intake (mL)
Time (hours)
Vehicle
DAU5884

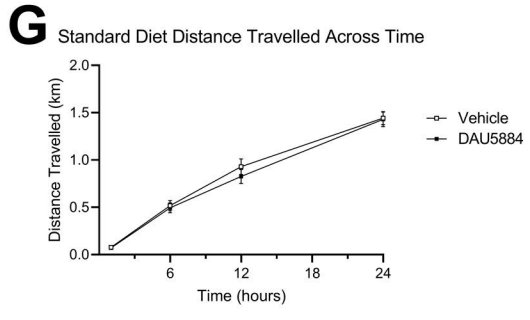
G
Standard Diet Distance Travelled Across Time
Distance Travelled (km)
Time (hours)
Vehicle
DAU5884

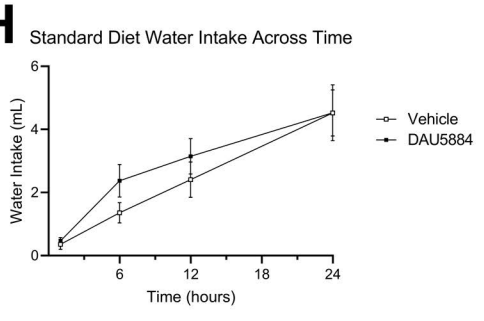
H
Standard Diet Water Intake Across Time
Water Intake (mL)
Time (hours)
Vehicle
DAU5884

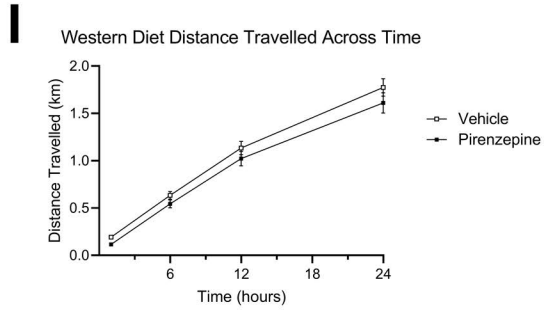
I
Western Diet Distance Travelled Across Time
Distance Travelled (km)
Time (hours)
Vehicle
Pirenzepine

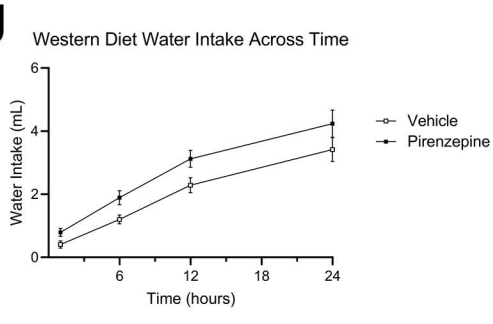
J
Western Diet Water Intake Across Time
Water Intake (mL)
Time (hours)
Vehicle
Pirenzepine

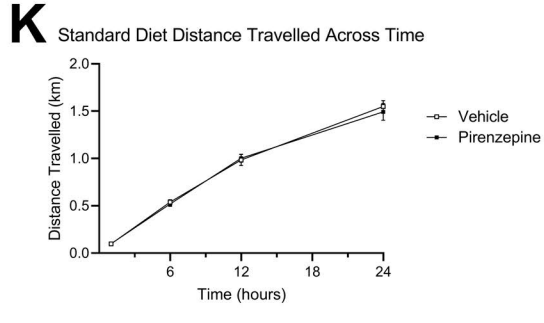
K
Standard Diet Distance Travelled Across Time
Distance Travelled (km)
Time (hours)
Vehicle
Pirenzepine

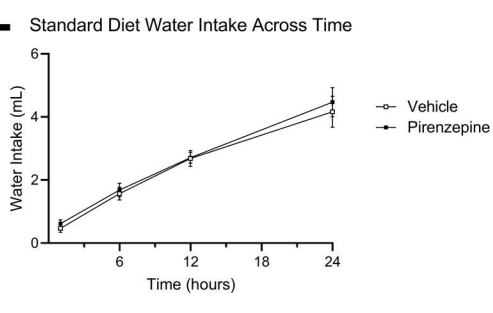
L
Standard Diet Water Intake Across Time
Water Intake (mL)
Time (hours)
Vehicle
Pirenzepine

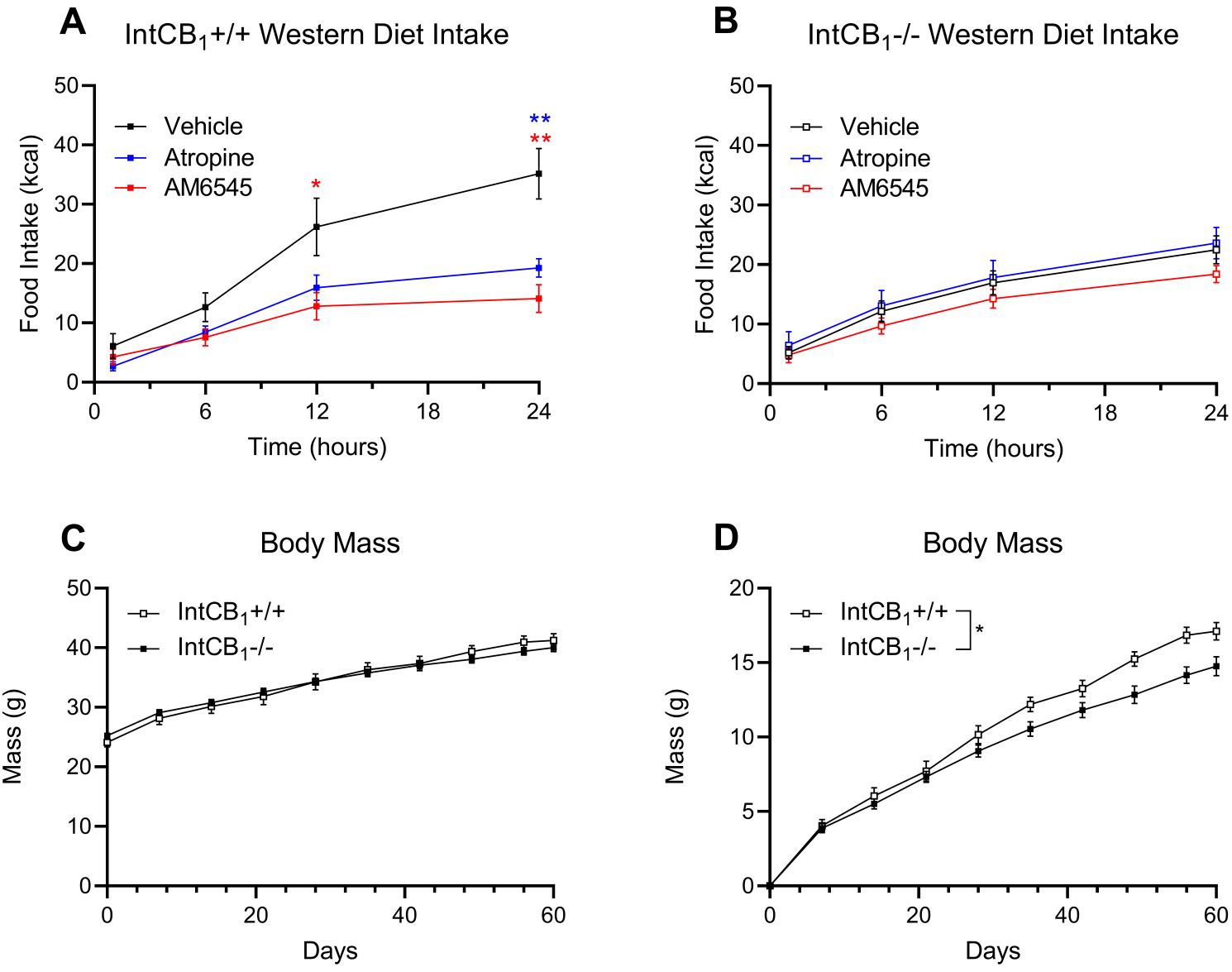
A
IntCB1+/+ Western Diet Intake
Food Intake (kcal)
Time (hours)
Vehicle
Atropine
AM6545
*
**
**
B
IntCB1-/- Western Diet Intake
Food Intake (kcal)
Time (hours)
Vehicle
Atropine
AM6545
C
Body Mass
Mass (g)
Days
IntCB1+/+
IntCB1-/-
D
Body Mass
Mass (g)
Days
IntCB1+/+
IntCB1-/-
*

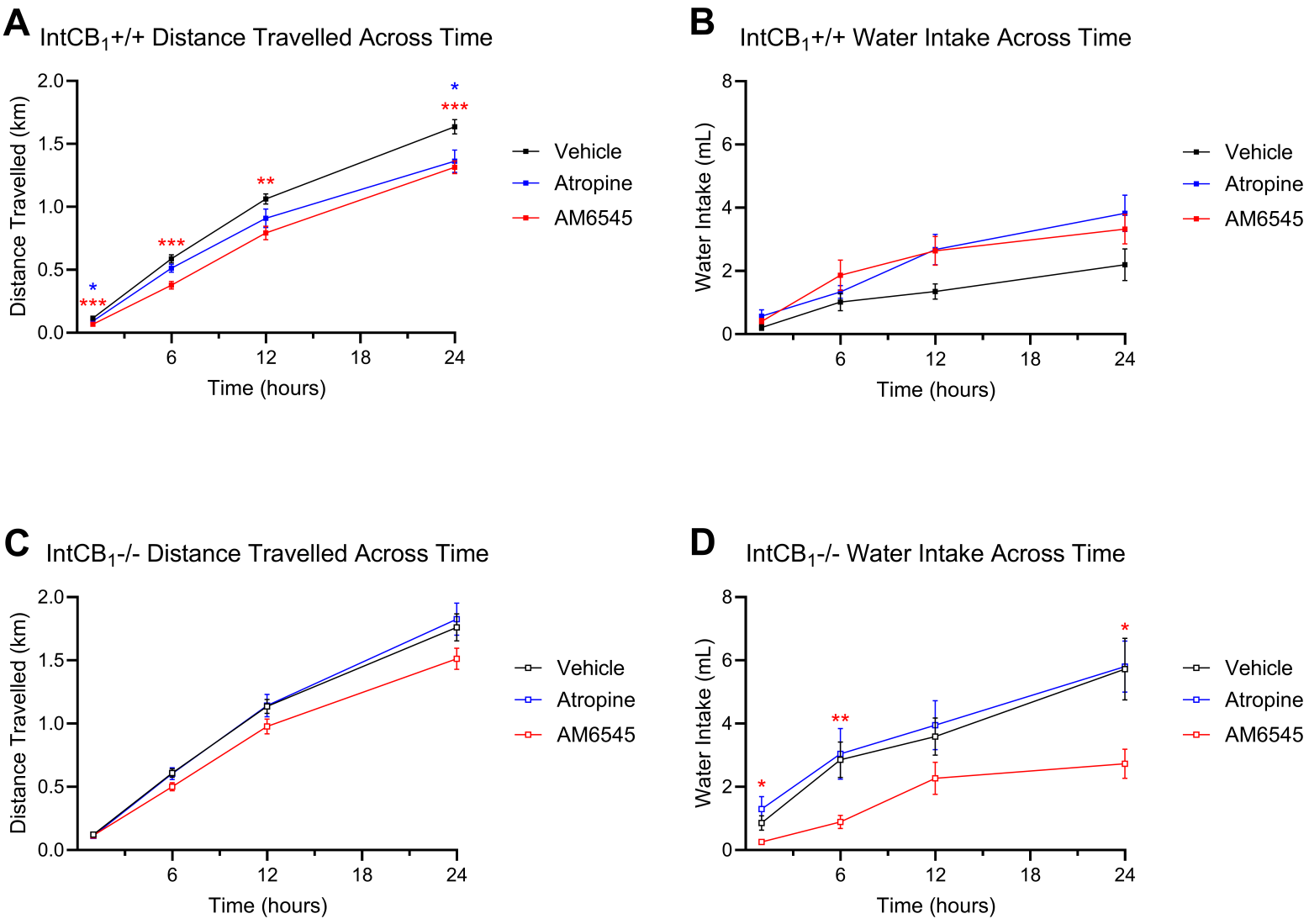
A
IntCB1+/+ Distance Travelled Across Time
Distance Travelled (km)
Time (hours)
Vehicle
Atropine
AM6545
B
IntCB1+/+ Water Intake Across Time
Water Intake (mL)
Time (hours)
Vehicle
Atropine
AM6545
C
IntCB1-/- Distance Travelled Across Time
Distance Travelled (km)
Time (hours)
Vehicle
Atropine
AM6545
D
IntCB1-/- Water Intake Across Time
Water Intake (mL)
Time (hours)
Vehicle
Atropine
AM6545

Table 1, 2-Way ANOVA table				
Figure	**Factor**	**F (DFn, DFd)**	**P value**	**Multiple Comparisons**
A	Time	F (1.370, 75.35) = 756.4	P<0.0001	n/a
	Drug	F (3, 55) = 5.875	P=0.0015	1 hr: Vehicle vs. ATR p = 0.0107, Vehicle vs. AM6545 p = 0.0020, Vehicle vs. both p < 0.0001; 6 hr: Vehicle vs. AM6545 p = 0020, Vehicle vs. Both p = 0.000; 12 hr: Vehicle vs. AM6545 p = 0.0392, Vehicle vs. Both p = 0.0002
	Time x Drug	F (9, 165) = 1.851	P=0.0628	n/a
B	Time	F (1.576, 83.01) = 95.51	P<0.0001	n/a
	Drug	F (3, 54) = 0.6320	P=0.5957	n/a
	Time x Drug	F (9, 158) = 0.6299	P=0.7703	n/a
C	Time	F (1.119, 61.57) = 344.2	P<0.0001	n/a
	Drug	F (3, 56) = 7.496	P=0.0003	1 hr: Vehicle vs. Both p = 0.0002; 6 hr: Vehicle vs. Both p < 0.0001; 12 hr: Vehicle vs. AM6545 p = 0.0061, Vehicle vs. Both p < 0.0001; 24 hr: Vehicle vs. Both p < 0.0001
	Time x Drug	F (9, 165) = 2.268	P=0.0202	n/a
D	Time	F (1.617, 86.79) = 131.9	P<0.0001	n/a
	Drug	F (3, 56) = 0.9563	P=0.4156	n/a

	Time x Drug	F (9, 161) = 0.5702	P=0.8201	n/a
E	Time	F (1.435, 39.70) = 568.4	P<0.0001	n/a
	Drug	F (1, 28) = 1.086	P=0.3063	n/a
	Time x Drug	F (3, 83) = 0.5128	P=0.6746	n/a
F	Time	F (1.632, 42.97) = 44.24	P<0.0001	n/a
	Drug	F (1, 28) = 5.920	P=0.0216	n/a
	Time x Drug	F (3, 79) = 3.963	P=0.0110	n/a
G	Time	F (2.070, 46.91) = 443.1	P<0.0001	n/a
	Drug	F (1, 24) = 0.3746	P=0.5462	n/a
	Time x Drug	F (3, 68) = 0.5729	P=0.6347	n/a
H	Time	F (1.455, 33.47) = 46.34	P<0.0001	n/a
	Drug	F (1, 24) = 0.4416	P=0.5127	n/a
	Time x Drug	F (3, 69) = 0.5618	P=0.6420	n/a
I	Time	F (1.377, 38.10) = 456.1	P<0.0001	n/a
	Drug	F (1, 28) = 2.280	P=0.1423	n/a
	Time x Drug	F (3, 83) = 0.4852	P=0.6935	n/a
J	Time	F (1.587, 40.73) = 147.1	P<0.0001	n/a

	Drug	F (1, 27) = 1.323	P=0.2601	n/a
	Time x Drug	F (3, 77) = 0.4454	P=0.7212	n/a
K	Time	F (1.643, 43.27) = 576.4	P<0.0001	n/a
	Drug	F (1, 28) = 0.2601	P=0.6141	n/a
	Time x Drug	F (3, 79) = 0.2981	P=0.8267	n/a
L	Time	F (1.421, 36.94) = 108.9	P<0.0001	n/a
	Drug	F (1, 27) = 0.2764	P=0.6033	n/a
	Time x Drug	F (3, 78) = 0.1415	P=0.9348	n/a

Table 2, 2-Way ANOVA table				
Figure	**Factor**	**F (DFn, DFd)**	**P value**	**Multiple Comparisons**
A	Time	F (1.702, 48.23) = 1085	P<0.0001	n/a
	Drug	F (2, 30) = 6.958	P=0.0033	1 hr: Vehicle vs. AM6545 p = 0.0002, Vehicle vs. ATR p = 0.0455, 6 hr: Vehicle vs. AM6545 p = 0.0002, 12 hr: Vehicle vs. AM6545 p = 0.0025, 24 hr: Vehicle vs. AM6545 p = 0.0008, Vehicle vs. ATR p = 0.0195
	Time x Drug	F (6, 85) = 4.619	P=0.0004	n/a
B	Time	F (1.292, 56.85) = 616.7	P<0.0001	n/a
	Drug	F (2, 45) = 2.272	P=0.1148	n/a
	Time x Drug	F (6, 132) = 2.082	P=0.0595	n/a
C	Time	F (2.130, 58.94) = 74.59	P<0.0001	n/a
	Drug	F (2, 29) = 2.217	P=0.1271	n/a
	Time x Drug	F (6, 83) = 1.707	P=0.1296	n/a
D	Time	F (1.849, 80.75) = 68.67	P<0.0001	n/a
	Drug	F (2, 45) = 3.398	P=0.0422	1 hr: Vehicle vs. AM6545 p = 0.0493, 6 hr: Vehicle vs. AM6545 p = 0.0081, 24 hr: Vehicle vs. AM6545 p = 0.0230
	Time x Drug	F (6, 131) = 2.619	P=0.0197	n/a